Hindawi
Structural Control and Health Monitoring
Volume 2023, Article ID 6648638, 23 pages
https://doi.org/10.1155/2023/6648638

WILEY | Hindawi

Research Article

Enhancements of Nonlinear Substructuring Control for Shake Table Experiments on Severely Damaged Structures

Ryuta Enokida[1] **and Koichi Kajiwara**[2]

[1]*International Research Institute of Disaster Science, Tohoku University, Sendai 980-0845, Japan*
[2]*E-Defense, National Research Institute for Earth Science and Disaster Resilience, 1501-21 Nishikameya Mitsuda, Shijimi-cho Miki, Hyogo 673-0515, Japan*

Correspondence should be addressed to Ryuta Enokida; enokida@irides.tohoku.ac.jp

Received 19 January 2023; Revised 4 May 2023; Accepted 18 May 2023; Published 6 June 2023

Academic Editor: Tzu-Kang Lin

This study introduces enhancements for nonlinear substructuring control (NLSC) to achieve simultaneous control of acceleration and displacement in shake table substructuring experiments with severely damaged structures. Although shake table control is greatly affected by a specimen placed on its top and its nonlinear characteristics, accurate control, even with nonlinear characteristics, is essential for experimental purposes. The NLSC was developed for a dynamically substructured system (DSS) scheme involving nonlinear substructures, and its first application to a shake table experiment was performed on a one-storey steel frame. In the experiment, NLSC realised simultaneous control of table acceleration and displacement with a slight nonlinear characteristic within the frame, although its performance degraded as the nonlinearity became stronger. To address this degradation issue, this study introduces two techniques for enhancing NLSC shake table substructuring experiments. One is a composite filtering technique to minimise noise-contaminating displacement data fed back to the table control so that the error feedback action in NLSC can be fully utilised. The other involves a new linear model that is assumed to be more highly damped than the actual system to enhance the stability robustness of NLSC against nonlinear characteristics. After a series of numerical examinations, this study experimentally examined the enhancements on actual shake table experiments using a steel frame. Using the NLSC with the enhancements, a substructuring experiment was successfully conducted; moreover, the NLSC realised simultaneous control of the table acceleration and displacement with nearly 100% accuracy, even with severe nonlinear characteristics.

1. Introduction

A shake table is a key experimental facility for earthquake engineering that examines the seismic performance of structural buildings or civil infrastructure [1]. For this examination, the facility is expected to excite the structures as per seismic records of actual events in the past or data synthesised for anticipated future events. However, some of these structures are so large that full-scale specimens cannot be placed on the table and directly excited by the facility. In such cases, a dynamic substructuring experimental approach is an effective alternative [2]. In this approach, the full-sized specimen to be tested, rephrased as an emulate system in this study, is divided into numerical and physical substructures that are simulated in the physical and numerical domains, respectively. In general, the core part of the emulate system is employed as the physical substructure, and the remainder is simulated as the numerical substructure.

When a dynamic substructuring experiment is performed using a shake table, the table control becomes more complicated than that in a conventional shake table experiment [3]. In shake table experiments, in general, specimens placed on top are expected to display nonlinear characteristics owing to structural failures for experimental purposes [4]. The appearance of such characteristics during the experiment is undesirable in controlling the shake table, resulting in the deterioration of control accuracy and prompting the occurrence of

instability [5–8]. Therefore, its improvement has been investigated by the application of many control methods, such as minimal control synthesis [9–11], which is a type of model-reference adaptive control [12], model-based control [13–15], and robust control designs [16, 17]. To solve this issue of nonlinearity, we developed a nonlinear signal-based control (NSBC) [18, 19] method that accurately controls a nonlinear system by utilising a nonlinear signal obtained from the outputs of the system and its linear model under the same input signal. In its application to a single-axis shake table experiment with a steel structure [8, 20], NSBC has achieved a seismic acceleration record on the table with nearly 100% accuracy, despite the structure displaying severe nonlinear characteristics owing to its structural damage. Its applications have been actively extended to more complicated issues with severe nonlinear characteristics [21–23].

With advancements in control methods, a shake table substructuring experiment is a viable option for evaluation of seismic performance of large or heavy structures that exceed the limitations of experimental apparatuses. Currently, shake table substructuring experiments are being actively investigated for earthquake engineering purposes [24–29]. To perform the substructuring experiment, two schemes can be used for achieving real-time interaction between the physical and numerical domains. One is a hybrid simulation (HS) scheme, whose original idea was proposed in the 1960s in Japan for earthquake and structural engineering purposes [30–32], and the other is a dynamically substructured system (DSS) scheme, which was developed from a control engineering perspective in the mid-2000s [33].

Many substructuring experiments in earthquake engineering have been performed using a class of HS schemes because of their historical background and simplicity. In this scheme, the actuation system is solely handled as its controlled system, simply using the output signal of a numerical substructure as the control input signal for the physical substructure. This simple feature is derived from the development of the pseudodynamical substructuring technique [32, 34–36], in which much time is given to operators to manually control the actuator. The success of this technique has encouraged the direct application of HS to dynamic substructuring experiments [37, 38]. Unlike the pseudoexperiment, the dynamic experiment is significantly affected by the dynamics of the controlled system, including actuation systems, in terms of its control performance and stability. In stability analyses [39–42], a pure time delay, which inherently exists in a controlled dynamical system, was found to prompt instability and degrade the reliability of the experiment, especially when the controlled system is lightly damped. To address this, various compensation approaches for the delay have been contrived to enhance the stability and control performance [39, 40, 43–45], and they have been applied to many HS substructuring experiments even with advanced control methods [46, 47].

The DSS scheme, which was developed from a control perspective, is another approach for achieving real-time interaction between the numerical and physical domains in dynamic substructuring experiments [33, 48, 49]. Unlike HS, DSS regards the set of two substructures and actuation systems as the controlled system, and its controllers are designed to minimise the error between the two signals of the substructures. Because of this feature, the stability and control performance of DSS are more robust against pure time delay than those of HS [42, 50]. Thus, DSS does not require delay compensation, which is fundamental to HS. However, because of the nature of DSS, its performance is more susceptible to the structural conditions of substructures than that of HS. Thus, various control methods (e.g., minimal control synthesis [33], model predictive control [51], and robust control theory [52]) have been employed to enhance the performance of DSS with nonlinear substructures, although linear substructuring control (LSC) has been proposed as the basic control method of DSS [33].

To address this issue, a nonlinear substructuring control (NLSC) [53, 54] was developed by introducing NSBC [18] into the LSC. As NLSC directly succeeds the features and benefits of NSBC, it also relies on linear models of the substructures for the generation of the nonlinear signal and its controller design. NLSC controllers can also be designed with transfer functions, even for controlling nonlinear systems, and their stability can be approximately analysed by stability theorems established for classical control theory. Thus far, the effectiveness and practicality of NLSCs have been well demonstrated by actual dynamic substructuring experiments using hydraulic actuators [53, 54]. Currently, the application of NLSC to a shake table is an important subject because the introduction of the basic DSS scheme to a shake table is susceptible to nonlinear characteristics [55].

In addition, shake table substructuring experiments require simultaneous control of the table acceleration and displacement to ensure device functionality and satisfy the requirements regarding the nature of the experiment [24, 27, 56]. When NLSC was first applied to a shake table [56], simultaneous control with nonlinear substructures was achieved. However, deterioration of its control performance was observed when the substructures displayed severe nonlinear characteristics. This application highlighted the necessity to improve the stability robustness of NLSC and enhance its control performance for controlled systems with severe parameter variations.

A possible solution is to increase the contribution of the error feedback action in NLSC because it leads to the error reduction when stability is maintained. However, there are two concerns for increasing the contribution: one is increasing the influence of noise contaminating the error signal on its control performance, and the other is stability robustness.

To resolve these two problems, this study introduces two techniques: noise reduction in the error signal and a new linear model design to improve the stability robustness of NLSC. The noise reduction technique introduced in this study is based on a composite filtering technique [57, 58] that minimises noise in displacement

data by the fusion of table displacement and acceleration data. In the new design, a linear model is intentionally designed to be more highly damped than the actual controlled system. This design is motivated by the nature of damping elements, which contributes to stabilisation, and the feature of NLSC, which allows a linear model to be flexibly designed because it relies on the model rather than the controlled system itself. This study numerically and experimentally examines these enhancements via shake table substructuring experiments with severe nonlinear characteristics.

The remainder of this paper is organised as follows. Section 2 describes the essence of the NLSC shake table experiments, its stability analysis, and the details of the enhancements proposed in this study. Section 3 numerically examines the enhancements of the NLSC shake table substructuring experiment. Section 4 presents experimental examinations of the enhancements via substructuring experiments with a physical substructure consisting of a single-degree-of-freedom (SDOF) structure and a single-axis shake table and a numerical 2DOF substructure with a nonlinear spring on each storey. Finally, Section 5 summarises the conclusions of this study.

2. NLSC for Shake Table Substructuring Experiments

Prior to detailing the enhancements for NLSC, the necessity of simultaneous control of table acceleration and displacement is exemplified using a shake table substructuring experiment on an emulate system, as shown in Figure 1.

The emulate system with N storeys in Figure 1(a) is described by the following equation:

$$m_{ei}\ddot{y}_{ei}(t) + f_{ei}(t) - f_{ei+1}(t) = 0 \quad (i = 1, \cdots, N), \tag{1}$$

where $f_{ei}(t)(= f_{eci}(t) + f_{eki}(t))$ is the resultant force of damping and restoring forces ($f_{eci}(t)$ and $f_{eki}(t)$) on the ith storey of the emulate system; $f_{eN+1}(t) = 0$; $\{y_{ei}, m_{ei}\}$ is the set of displacements and masses of the ith storey in the system, respectively. When substructures are built by dividing the system based on the qth storey, its upper part (the qth to Nth storeys) becomes a part of the physical substructure, whereas the lower part (the 1st to $q-1$th storeys) becomes the numerical substructure, as shown in Figure 1(b). The upper and lower parts of the emulate system are described as follows:

$$\left\{\begin{array}{c} m_{eN}\left(\ddot{y}_{eN}(t) - \ddot{y}_{eq-1}(t)\right) + f_{eN}(t) = -m_{eN}\ddot{y}_{eq-1}(t), \\ m_{eN-1}\left(\ddot{y}_{eN-1}(t) - \ddot{y}_{eq-1}(t)\right) + f_{eN-1}(t) - f_{eN}(t) = -m_{eN-1}\ddot{y}_{eq-1}(t), \\ \vdots \\ m_{eq}\left(\ddot{y}_{eq}(t) - \ddot{y}_{eq-1}(t)\right) + f_{eq}(t) - f_{eq+1}(t) = -m_{eq}\ddot{y}_{eq-1}(t), \end{array}\right\} \tag{2a}$$

$$\left\{\begin{array}{c} m_{eq-1}\ddot{y}_{eq-1}(t) + f_{eq-1}(t) - f_{eq}(t) = 0, \\ \vdots \\ m_{e2}\ddot{y}_{e2}(t) + f_{e2}(t) - f_{e3}(t) = 0, \\ m_{e1}\ddot{y}_{e1}(t) + f_{e1}(t) - f_{e2}(t) = 0. \end{array}\right\}. \tag{2b}$$

Equation (2a): the upper part of the emulate system (i.e., the qth to Nth storeys).

Equation (2b): the lower part of the emulate system (i.e., the 1st to $q-1$th storeys).

In equation (2), the acceleration on the $q-1$ storey, $\ddot{y}_{eq-1}(t)$, acts on all the storeys in the upper part as an external excitation. In addition, the interactive force between the upper and lower parts (i.e., f_{eq}) is a function described by the following equation:

$$f_{eq}(t) = F\left(\dot{y}_{eq}(t), \dot{y}_{eq-1}(t), y_{eq}(t), y_{eq-1}(t)\right). \tag{3}$$

A shake table substructuring experiment for the emulate system is executed using the set of numerical and physical

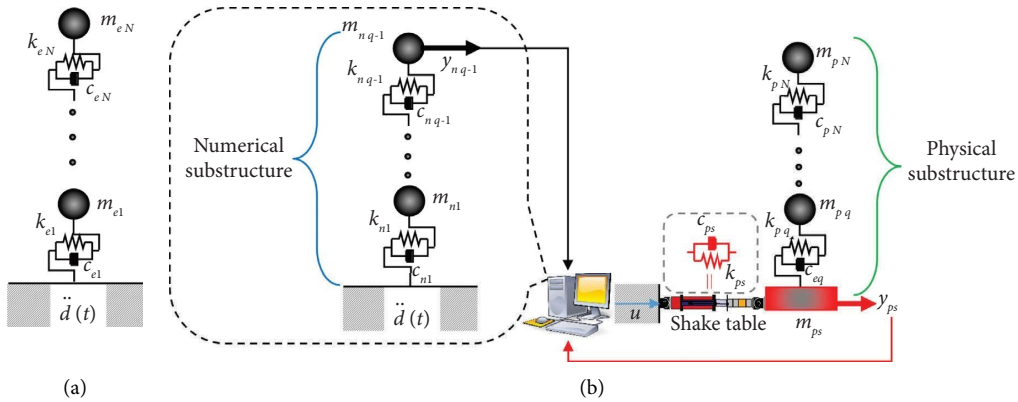

FIGURE 1: Shake table substructuring experiment for an emulate system: (a) emulate system having N storeys and (b) substructures with shake table.

substructures including a shake table, whose equations of motion are described as follows:

$$\left\{\begin{array}{c} m_{pN}\left(\ddot{y}_{pN}(t)-\ddot{y}_{ps}(t)\right)+f_{pN}(t)=-m_{pN}\ddot{y}_{ps}(t), \\ m_{pN-1}\left(\ddot{y}_{pN-1}(t)-\ddot{y}_{ps}(t)\right)+f_{pN-1}(t)-f_{pN}(t)=-m_{pN-1}\ddot{y}_{ps}(t), \\ \vdots \\ m_{pq}\left(\ddot{y}_{pq}(t)-\ddot{y}_{ps}(t)\right)+f_{pq}(t)-f_{pq+1}(t)=-m_{pq}\ddot{y}_{ps}(t), \\ m_{ps}\ddot{y}_{ps}(t)+c_{ps}\dot{y}_{ps}(t)+k_{ps}y_{ps}(t)-f_{pq}(t)=k_{ps}u(t), \end{array}\right\}, \tag{4a}$$

$$\left\{\begin{array}{c} m_{nq-1}\ddot{y}_{nq-1}(t)+f_{nq-1}(t)-f_{nq}(t)=0, \\ \vdots \\ m_{n2}\ddot{y}_{n2}(t)+f_{n2}(t)-f_{n3}(t)=0, \\ m_{n1}\ddot{y}_{e1}(t)+f_{n1}(t)-f_{n2}(t)=0. \end{array}\right\}. \tag{4b}$$

Equation (4a): physical substructure consisting of a shake table and specimen (corresponding to the upper part of the emulate system).

Equation (4b): numerical substructure (corresponding to the lower part of the emulate system).

In equation (4), $\{y_{pi}, m_{pi}, f_{pi}(=f_{pci}+f_{pki}), (i=q,\ldots,N)\}$, and $\{y_{ni}, m_{ni}, f_{ni}(=f_{nci}+f_{nki}), (i=1,\ldots,q-1)\}$ are the sets of the displacement, mass, and resultant force (derived from the damping and restoring forces) of the physical and numerical substructures corresponding to the ith storey of the emulate system, respectively; $\{y_{ps}, m_{ps}, c_{ps}, k_{ps}\}$ denotes the displacement, mass, damping coefficient, and stiffness of the shake table, respectively, when the table is equivalently modelled using a mass-spring-damper model; and u is the control input signal. It should be noted that as the dynamics of the shake table are significantly affected by the specimen on its top, the shake table is incorporated into the physical substructure to more directly consider the change in its dynamics.

Similar to the emulate system described by equation (2), equation (4) suggest that the shake table acceleration $\ddot{y}_{ps}(t)$ acts on all the storeys of the specimen as an external excitation. In addition, the interactive force $f_{pq}=(f_{nq})$ between the physical and numerical substructures is the function described by

$$f_{pq}(t)=F\left(\dot{y}_{pq}(t),\dot{y}_{ps}(t),y_{pq}(t),y_{ps}(t)\right). \tag{5}$$

According to the above formulations, the emulate system in equation (2) can be duplicated by the shake table substructuring experiment in equation (4), when $\ddot{y}_{ps}(t)=\ddot{y}_{eq-1}(t)$ and equation (3) = equation (5). In other words, the duplication can be achieved by realising the following condition:

$$\ddot{y}_{ps}(t)=\ddot{y}_{pq-1}(t),\ \dot{y}_{ps}(t)=\dot{y}_{pq-1}(t),\ y_{ps}(t)=y_{pq-1}(t). \tag{6}$$

Equation (6) clearly indicates the necessity of controlling the acceleration, velocity, and displacement of the shake table for accurate duplication. Thus, this study aims to simultaneously control table acceleration and displacement in substructuring experiments on severely damaged structures, based on the premise that the table velocity can be naturally controlled by the accurate simultaneous control of its displacement and acceleration. In practice, simultaneous

control is executed by feeding back the table acceleration and displacement for determining the control input signal.

This study realises the simultaneous control based on NLSC with enhancements. The principles of the NLSC and its stability analysis are briefly described in Section 2.1, and the enhancements are detailed in Section 2.2.

2.1. Principles of NLSC. NLSC was developed as a control approach, particularly for the DSS scheme involving nonlinear characteristics [53]. This scheme regards the set of actuation systems and substructures as the controlled system, unlike the HS scheme, where actuation systems are solely considered the controlled system. Owing to this difference, the signal flows and controller design of DSS become more complicated than those of HS. As NLSC was developed by incorporating the nonlinear control approach of NSBC into LSC, which is the basic control approach for DSS, it has features of both NSBC and DSS. Based on the form of DSS [33], the block diagram of NLSC for the shake table experiment is depicted in Figure 2.

Owing to the feature of NSBC, NLSC does not require accurate information on the structural conditions of substructures (e.g., nonlinear characteristics) for its controller design and practice as it relies on linear models of the substructures. Based on this feature, this study describes substructures with nonlinear characteristics using the transfer functions shown in Figure 2, although nonlinear systems cannot be described rigorously in such a manner.

2.1.1. Controller Design of NLSC. According to Figure 2, the output signals of the physical and numerical substructures y_{ps} and y_{nq-1} are described by

$$\begin{cases} y_{ps}(s) = G_{ps}(s)e^{-\tau s}u(s), \\ y_{nq-1}(s) = U_{nq-1}(s)\big(G_d(s)d(s) - y_{ps}(s)\big), \end{cases} \tag{7}$$

where τ is the pure time delay; d is the external disturbance; $G_{ps}(s)$ is the table dynamic in the physical substructure; $U_{nq-1}(s)$ is the dynamics of the top (i.e., $q-1$) storey in the numerical substructure; and $G_d(s)$ is the dynamics associated with the external disturbance. The outputs of these linear models are described by

$$\begin{cases} \overline{y}_{ps}(s) = \overline{G}_{ps}(s)e^{-\overline{\tau}s}u(s), \\ \overline{y}_{nq-1}(s) = \overline{U}_{nq-1}(s)\big(\overline{G}_d(s)d(s) - \overline{y}_{ps}(s)\big). \end{cases} \tag{8}$$

Note that this study describes a linear model of X or its parameter x using $\overline{X}$ or $\overline{x}$. In addition, $\overline{\tau}$ in equation (8) is the estimate of the pure time delay used with the physical linear model.

NLSC handles the difference between a controlled system and its linear model as a nonlinear characteristic, regardless of the presence of nonlinear elements in the controlled system. According to Figure 2, the nonlinear characteristics can be measured as a nonlinear signal, which is obtained using

$$\sigma(s) = \sigma_n(s) - \sigma_p(s), \tag{9}$$

where $\sigma_n(s)(= y_{nq-1}(s) - \overline{y}_{nq-1}(s))$ and $\sigma_p(s)(= y_{ps}(s) - \overline{y}_{ps}(s))$ are the nonlinear signals associated with physical and numerical substructures, respectively. In addition, the set of nonlinear signals and error signal: $e(s)(= y_{nq-1}(s) - y_{ps}(s))$ is described by

$$\begin{cases} \sigma_n(s) = S_{n1}(s)d(s) - S_{n2}(s)\overline{G}_p(s)e^{-\overline{\tau}s}u(s) - S_{n3}(s)\sigma_p(s), \\ \sigma_p(s) = S_p(s)\overline{G}_{ps}(s)e^{-\overline{\tau}s}u(s), \\ e(s) = \overline{U}_d(s)d(s) - \overline{U}_u(s)e^{-\overline{\tau}s}u(s) + \sigma(s), \end{cases} \tag{10}$$

where $S_p(s) = (1 + \Delta G_{ps}(s)/\overline{G}_{ps}(s))e^{-\Delta\tau s} - 1$; $\Delta G_{ps}(s) = G_{ps}(s) - \overline{G}_{ps}(s)$; $\Delta\tau = \tau - \overline{\tau}$; $S_{n1}(s) = U_{nq-1}(s)G_d(s) - \overline{U}_{nq-1}(s)\overline{G}_d(s)$, $S_{n2}(s) = U_{nq-1}(s) - \overline{U}_{nq-1}(s)$; $S_{n3}(s) = U_{nq-1}(s)$; $\overline{U}_d(s) = \overline{U}_{nq-1}(s)\overline{G}_d(s)$; and $\overline{U}_u(s) = (\overline{U}_{nq-1}(s) + 1)\overline{G}_{ps}(s)$.

The NLSC uses these signals to determine the control input signal u, which is obtained using

$$u(s) = K_d(s)d(s) + K_e(s)e(s) + K_\sigma(s)\sigma(s), \tag{11}$$

where $\{K_d(s), K_e(s), K_\sigma(s)\}$ is the set of controllers acting on the signals of $\{d, e, \sigma\}$. By substituting equations (11) into (10), the error signal becomes

$$e(s) = \frac{\overline{U}_d(s) - \overline{U}_u(s)e^{-\overline{\tau}s}K_d(s)}{1 + \overline{U}_u(s)e^{-\overline{\tau}s}K_e(s)}d(s) + \frac{1 - \overline{U}_u(s)e^{-\overline{\tau}s}K_\sigma(s)}{1 + \overline{U}_u(s)e^{-\overline{\tau}s}K_e(s)}\sigma(s). \tag{12}$$

In the previous studies on NLSC [53, 54, 56], the following controllers have been effective in minimising the error in equation (12) particularly when $\Delta\tau = 0$:

$$\begin{aligned} K_d(s) &= \frac{\overline{U}_d(s)}{\overline{U}_u(s)}F_d(s), \\ K_e(s) &= \frac{1}{\overline{U}_u(s)}F_e(s), \\ K_\sigma(s) &= \frac{1}{\overline{U}_u(s)}F_\sigma(s), \end{aligned} \tag{13}$$

where $\{F_d(s), F_e(s), F_\sigma(s)\}$ is the set of filters associated with the controllers of $\{K_d(s), K_e(s), K_\sigma(s)\}$.

2.1.2. Stability Analysis. When $G(s)$ is given somehow, the stability of the NLSC shake table substructuring experiment is governed by the feedback signals [56], which are described by

$$\begin{bmatrix} \sigma_n(s) \\ \sigma_p(s) \\ e(s) \end{bmatrix} = \mathbf{J}(s)^{-1}\mathbf{J}_0(s)\mathrm{d}(s), \tag{14}$$

where

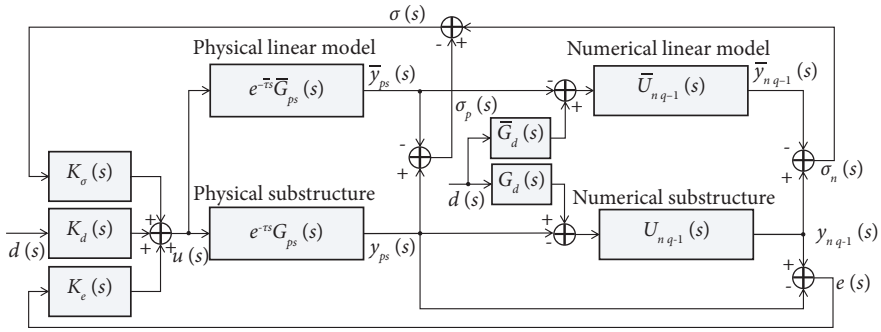

Figure 2: NLSC for shake table substructuring experiments.

$$\mathbf{J}(s)=\begin{bmatrix} S_p(s)\overline{G}_{ps}(s)K_\sigma(s)e^{-\bar{\tau}s} & -\left(1+S_p(s)\overline{G}_{ps}(s)K_\sigma(s)e^{-\bar{\tau}s}\right) & S_p(s)\overline{G}_{ps}(s)K_e(s)e^{-\bar{\tau}s} \\ 1+S_{n2}(s)\overline{G}_{ps}(s)K_\sigma(s)e^{-\bar{\tau}s} & S_{n3}(s)-S_{n2}(s)\overline{G}_{ps}(s)K_\sigma(s)e^{-\bar{\tau}s} & S_{n2}(s)\overline{G}_{ps}(s)K_e(s)e^{-\bar{\tau}s} \\ -\left(1-\overline{U}_u(s)K_\sigma(s)e^{-\bar{\tau}s}\right) & 1-\overline{U}_u(s)K_\sigma(s)e^{-\bar{\tau}s} & 1+\overline{U}_u(s)K_e(s)e^{-\bar{\tau}s} \end{bmatrix}, \tag{15}$$

and $\mathbf{J_0}(s)=\begin{bmatrix} -S_p(s)\overline{G}_{ps}(s)K_d(s)e^{-\bar{\tau}s} \\ S_{n1}(s)-S_{n2}(s)\overline{G}_{ps}(s)K_d(s)e^{-\bar{\tau}s} \\ \overline{U}_d(s)-\overline{U}_u(s)K_d(s)e^{-\bar{\tau}s} \end{bmatrix}$. Determinant of $\mathbf{J}(s)$: $\det(\mathbf{J}(s))$, which is the closed-loop characteristic equation of (14) can be described as follows:

$$\begin{aligned} L(s)&\left(=\det\left(\mathbf{J}(s)\right)=1+H_\tau(s)=1+H(s)e^{-\bar{\tau}s}\right) \\ &=1+e^{-\bar{\tau}s}\left[\overline{U}_u(s)K_e(s)+\left(S_{n3}(s)S_p(s)+S_{n2}(s)+S_p(s)\right)\overline{G}_{ps}(s)\left(K_\sigma(s)+K_e(s)\right)\right]. \end{aligned} \tag{16}$$

Stability can be assessed by applying the Nyquist stability criterion, which is commonly used for the stability analysis of a system with a pure time delay, to equation (16). This stability analysis requires visual assessment by counting the number of Nyquist plot encirclements of the critical point ($-1+0{\cdot}j$, where $j=(-1)^{1/2}$) in the complex plane. However, this assessment has difficulty in assessing unstable systems or conditionally stable systems, particularly when the systems have many encirclement near the critical point. To address this issue, an equivalent approach has recently been proposed for systematically calculating encirclements without relying on the visual assessment of the original approach [56]. In this study, the stability is analysed using this equivalent approach.

2.2. Enhancements of NLSC. According to equation (16), the stability of NLSC is affected by the properties of both the numerical and physical substructures, as well as those of the linear models. Nonlinear characteristics in substructures occasionally cause instability, particularly when NLSC does not have sufficient stability robustness against parameter variations in the substructures. To perform reliable substructuring experiments even with severely damaged structures, NLSC must have sufficient stability robustness and accurate synthesis of the outputs of the substructures.

Therefore, this study increases the contribution of the error feedback action in NLSC, introducing two enhancements to reduce the noise amplification in the error signal and improve stability robustness. One enhancement is a highly damped linear model design that enhances its stability robustness against parameter variations in the substructures. The other is a composite filtering technique [57, 58] for noise reduction in the error signal.

2.2.1. Highly Damped Linear Model Design. In the highly damped linear model design, the damping coefficients in the linear model are intentionally designed to be larger than those of the actual controlled systems. This design was motivated by the natures of highly-damped systems and NSBC, which is the origin of NLSC. First, stability, in general, is greatly influenced by damping elements in the controlled system: a highly-damped system generally gains a larger stability margin than a low-damped system. Second, NSBC does not require accurate information on a controlled system and alternatively utilises its linear model, which has a modelling gap with the controlled system to a greater or lesser degree.

The new design intentionally enlarges the modelling gaps of the damping elements between the (numerical and physical) substructures and those linear models, and the gaps are treated as nonlinear dynamics to be handled by NLSC. In this design, the damping coefficients in the linear models become

$$\left\{\bar{c}_{n1},\ldots,\bar{c}_{nq-1},\bar{c}_{pq}\cdots,\bar{c}_{pN}\right\}=\left\{\gamma_{c1}\cdot c_{n1},\ldots,\gamma_{cN}\cdot c_{pq-1},\gamma_{cq}\cdot c_{pq}\cdots,\gamma_{cN}\cdot c_{pN}\right\}, \tag{17}$$

where $\gamma_{ci} > 1$ $(i = 1,\ldots,N)$.

2.2.2. Composite Filtering Technique for Acceleration and Displacement of Shake Table. The error feedback controller in the NLSC plays an important role in maintaining stability [56], and its conventional form is illustrated in Figure 3(a). Controller $K_e(s)$ using $F_e(s) = \omega_e^2/(s^2 + 2\omega_e s)$ is an effective design, according to various studies on NLSC [53, 54, 56]. In this design, a larger cut-off frequency ω_e contributes to reducing the error and maintaining stability, even with a wide range of parameter variations in the substructures. However, this cut-off frequency has been found to be associated with the noise amplification in the table displacement, and K_e with a high cut-off frequency resulted in a significantly large noisy acceleration [56]. To maintain stability over a wide range of parameter variations, we require an enhancement technique that allows us to assign a sufficiently large ω_e without causing noise amplification.

To mitigate the noise in the table displacement data, this study introduces the application of a composite filtering technique [57, 58], as shown in Figure 3(b), which generates new displacement data from the fusion of acceleration and displacement data. The new table displacement obtained by data fusion is expressed as follows:

$$\begin{aligned} y_{ps}^{c}(s)\left(=\frac{\omega_s y_{ps}(s)+s y_{ps}(s)}{s+\omega_s}\right) &= \frac{\omega_s}{s+\omega_s}y_{ps}(s)+\frac{s}{s+\omega_s}\frac{1}{s^2}\ddot{y}_{ps}(s) \\ &= K_{cf1}(s)y_{ps}(s)+K_{cf2}(s)\ddot{y}_{ps}(s), \end{aligned} \tag{18}$$

where $K_{cf1} = \omega_s/(s + \omega_s)$; $K_{cf2} = 1/(s^2 + \omega_s s)$; and ω_s is the switching frequency used to determine the contribution of the original acceleration and displacement data to the new data.

In this technique, the first term with K_{cf1} eliminates high-frequency components in the original displacement data, including noise, which is amplified by error feedback action. The second term with K_{cf2}, which is the double integration of acceleration data, compensates for the eliminated components. This complimentary relation of K_{cf1} and K_{cf2} is evident from equation (18). Thus, this technique can mitigate the noise for the new displacement without causing any phase lag, which appears as some delay in time history data. Then, a high cut-off frequency can be assigned to controller K_e with relief from the noise amplification issue, and the designed controller can enhance the stability robustness.

3. Numerical Examination of NLSC

The enhancements are numerically examined by a series of NLSC shake table substructuring tests on an emulate 3DOF system. This system is divided into a numerical 2DOF substructure and a physical substructure, which consists of an SDOF specimen and a shake table, as shown in Figure 4.

In this study, a shake table without any specimens is modelled using the following second-order transfer function, as it is commonly employed for modelling and easily changed to an equivalent mass-spring-damper model:

$$\begin{aligned} G_{ps}\left(=\frac{y_{ps}(s)}{u(s)}\right) &= \frac{\omega_{ps0}^2}{s^2+2\zeta_{ps0}\omega_{ps0}s+\omega_{ps0}^2} \\ &= \frac{k_{ps0}}{m_{ps0}s^2+c_{ps0}s+k_{ps0}}, \end{aligned} \tag{19}$$

where $\{\omega_{ps0}, \zeta_{ps0}, m_{ps0}(= m_{ps}), c_{ps0}, k_{ps0}\}$ is the set of natural circular frequency, damping ratio, mass, equivalent damping coefficient, and equivalent stiffness, respectively, of the shake table without a specimen. This modelling is practical for describing table dynamics in the time domain, and it can be easily extended to the modelling of a table with a specimen.

The substructuring formulation for Figure 4 and its NLSC controller design are described in Section 3.1, and the numerical conditions for the simulations are detailed in Section 3.2. The stability is analysed in Section 3.3, and the results of the substructuring tests with enhancements are described in Section 3.4.

3.1. Controller Design and Substructuring Form. The emulate 3DOF system is described as follows:

$$\begin{cases} m_{e3}\ddot{y}_{e3}(t)+f_{e3}(t)=0, \\ m_{e2}\ddot{y}_{e2}(t)+f_{e2}(t)=f_{e3}(t), \\ m_{e1}\ddot{y}_{e1}(t)+f_{e1}(t)=f_{e2}(t). \end{cases} \tag{20}$$

This emulate system is divided into a set of a numerical 2DOF substructure, and a physical substructure consisting of an SDOF specimen and shake table. The set of substructures is described by

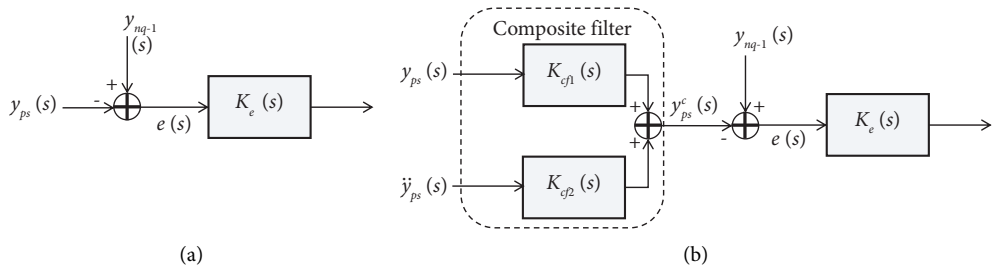

Figure 3: Error feedback actions: (a) conventional error signal and (b) composite filtered error signal.

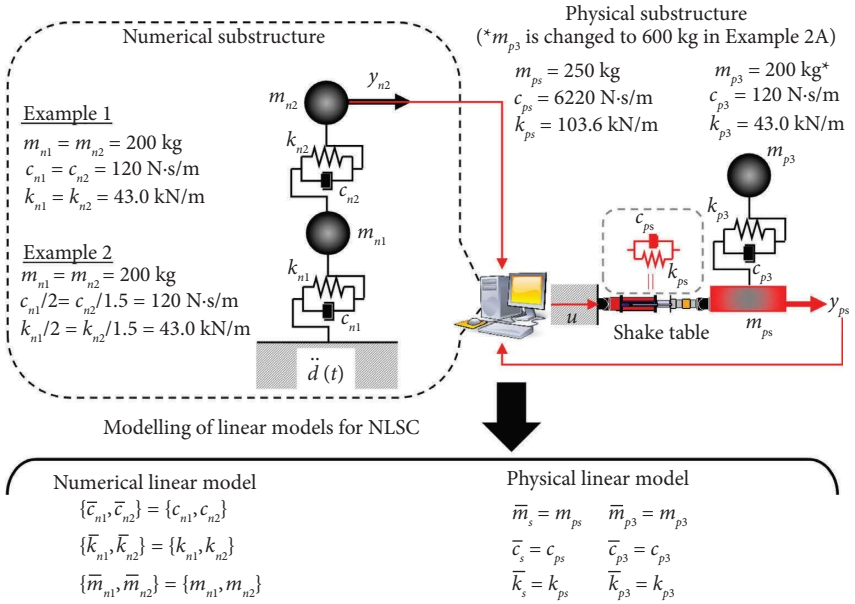

Figure 4: Numerical configurations for numerical 2DOF and physical SDOF substructures.

$$\begin{cases} m_{p3}\ddot{y}_{p3}(t) + f_{p3}(t) = 0, \\ m_{ps}\ddot{y}_{ps}(t) + c_{ps}\dot{y}_{ps}(t) + k_{ps}y_{ps}(t) - f_{p3}(t) = k_{ps}u(t), \\ m_{ni}\ddot{y}_{ni}(t) + f_{ni}(t) = f_{ni+1}(t) \quad (i = 1, 2), \end{cases} \tag{21}$$

where $\{m_{ps}, c_{ps}, k_{ps}\}$ is the set of mass, corresponding damping coefficient, and corresponding stiffness, respectively, of the table supporting a specimen; $\{y_{p3}, m_{p3}\}$ is the set of displacement and mass of the SDOF specimen; $\{y_{ni}, m_{ni}\}$ is the set of displacement and mass of the ith storey in the numerical substructure; and $f_{n3}(t) = f_{p3}(t)$.

For substructures in equation (21), those linear models are described by

$$\begin{cases} \overline{m}_{p3}\ddot{\overline{y}}_{p3}(t) + \overline{f}_{p3}(t) = 0, \\ \overline{m}_{ps}\ddot{\overline{y}}_{ps}(t) + \overline{c}_{ps}\dot{\overline{y}}_{ps}(t) + \overline{k}_{ps}\overline{y}_{ps}(t) - \overline{f}_{p3}(t) = \overline{k}_{ps}u(t), \\ \overline{m}_{ni}\ddot{\overline{y}}_{ni}(t) + \overline{f}_{ni}(t) = \overline{f}_{ni+1}(t) \quad (i = 1, 2), \end{cases} \tag{22}$$

where $\overline{f}_{p3}(t) = \overline{c}_{p3}(\dot{\overline{y}}_{p3}(t) - \dot{\overline{y}}_{p2}(t)) + \overline{k}_{p3}(\overline{y}_{p3}(t) - \overline{y}_{p2}(t))$; $\overline{y}_{p2}(t) = \overline{y}_{ps}(t)$; $\overline{f}_{ni}(t) = \overline{c}_{ni}(\dot{\overline{y}}_{ni}(t) - \dot{\overline{y}}_{ni-1}(t)) + \overline{k}_{ni}(\overline{y}_{ni}(t) - \overline{y}_{ni-1}(t))$ $(i = 1, 2)$; $\overline{f}_{n3}(t) = \overline{f}_{p3}(t)$; $\overline{y}_{n0}(t) = d(t)$; and $\{\overline{y}_{p3}, \overline{c}_{p3}, \overline{k}_{p3}\}$ are the set of displacement, damping, and stiffness of the linear model of the SDOF specimen, respectively.

According to NLSC controller design [56], the physical linear model in equation (22) can be transformed into the following transfer functions:

$$\begin{cases} \overline{G}_{p3}(s)\left(=\dfrac{\overline{y}_{p3}(s)}{\overline{y}_{p2}(s)}=\dfrac{\overline{y}_{p3}(s)}{\overline{y}_{ps}(s)}\right)=\dfrac{\overline{c}_{p3}s+\overline{k}_{p3}}{\overline{m}_{p3}s^2+\overline{c}_{p3}s+\overline{k}_{p3}}, \\ \overline{G}_{ps}(s)\left(=\dfrac{\overline{y}_{ps}(s)}{u(s)}\right)=\dfrac{\overline{k}_{ps}/\left(\overline{c}_{p3}s+\overline{k}_{p3}\right)}{\left(\overline{m}_{ps}s^2+\left(\overline{c}_{ps}+\overline{c}_{p3}\right)s+\overline{k}_{ps}+\overline{k}_{p3}\right)/\left(\overline{c}_{p3}s+\overline{k}_{p3}\right)-\overline{G}_{p3}(s)}. \end{cases} \tag{23}$$

Similarly, the numerical linear model in equation (22) is transformed into the following:

$$\begin{cases} \overline{G}_{n2}(s)\left(=\dfrac{\overline{y}_{n2}(s)}{\overline{y}_{n1}(s)}\right)=\dfrac{\overline{W}_0(s)}{1+\overline{V}_0(s)\overline{y}_{ps}(s)/\overline{y}_{n2}(s)}, \\ \overline{G}_{n1}(s)\left(=\dfrac{\overline{y}_{n1}(s)}{\overline{y}_{n0}(s)}=\dfrac{\overline{y}_{n1}(s)}{d(s)}\right)=\dfrac{\overline{V}_{n2}(s)}{\overline{W}_{n2}(s)-\overline{G}_{n2}(s)}, \end{cases} \tag{24}$$

where

$$\overline{W}_0(s)=\frac{\overline{c}_{n2}s+\overline{k}_{n2}}{\overline{m}_{n2}s^2+\overline{c}_{n2}s+\overline{k}_{n2}},$$

$$\overline{V}_0(s)=\frac{\left(\overline{c}_{p3}s+\overline{k}_{p3}\right)}{\left(\overline{m}_{n2}s^2+\overline{c}_{n2}s+\overline{k}_{n2}\right)}\left(1-\overline{G}_{p3}(s)\right), \tag{25}$$

$$\overline{W}_{n2}(s)=\frac{\overline{m}_{n1}s^2+\left(\overline{c}_{n2}+\overline{c}_{n1}\right)s+\overline{k}_{n2}+\overline{k}_{n1}}{\overline{c}_{n2}s+\overline{k}_{n2}},$$

$$\overline{V}_{n2}(s)=\frac{\overline{c}_{n1}s+\overline{k}_{n1}}{\overline{c}_{n2}s+\overline{k}_{n2}}.$$

Equation (24) can be rewritten as

$$\begin{cases} \overline{y}_{n2}(s)-\overline{W}_0(s)\overline{y}_{n1}(s)+\overline{V}_0(s)\overline{y}_{ps}(s)=0, \\ \overline{y}_{n2}(s)-\overline{W}_{n2}(s)\overline{y}_{n1}(s)+\overline{V}_{n2}(s)d(s)=0. \end{cases} \tag{26}$$

Based on equation (26), all the outputs of the numerical linear model are described by

$$\overline{\mathbf{Y}}_{\mathbf{n}}(s)=\overline{\mathbf{T}}(s)^{-1}\left(\overline{\mathbf{Q}}_{\mathbf{1}}(s)d(s)-\overline{\mathbf{Q}}_{\mathbf{2}}(s)\overline{y}_{ps}(s)\right), \tag{27}$$

where $\overline{\mathbf{T}}(s)=\begin{bmatrix}1 & -\overline{W}_0(s)\\ 1 & -\overline{W}_{n2}(s)\end{bmatrix}$; $\overline{\mathbf{Y}}_{\mathbf{n}}(s)=\begin{bmatrix}\overline{y}_{n2}(s)\\ \overline{y}_{n1}(s)\end{bmatrix}$; $\overline{\mathbf{Q}}_{\mathbf{1}}(s)=\begin{bmatrix}0\\ -\overline{V}_{n2}(s)\end{bmatrix}$; and $\overline{\mathbf{Q}}_{\mathbf{2}}(s)=\begin{bmatrix}\overline{V}_0(s)\\ 0\end{bmatrix}$. Subsequently, the output of the top part of the numerical linear model becomes

$$\begin{aligned}\overline{y}_{n2}(s)\left(=\overline{\mathbf{C}}_{\mathbf{s}}\overline{\mathbf{Y}}_{\mathbf{n}}(s)\right)&=\overline{U}_d(s)d(s)-\overline{U}_{n2}(s)\overline{y}_{ps}(s)\\ &=\overline{U}_{n2}(s)\left(\overline{G}_d(s)d(s)-\overline{y}_{ps}(s)\right),\end{aligned} \tag{28}$$

where $\overline{\mathbf{C}}_{\mathbf{s}}=\begin{bmatrix}1 & 0\end{bmatrix}$; $\overline{U}_d(s)=\overline{\mathbf{C}}_{\mathbf{s}}\overline{\mathbf{T}}(s)^{-1}\overline{\mathbf{Q}}_{\mathbf{1}}(s)$; $\overline{U}_{n2}(s)=\overline{\mathbf{C}}_{\mathbf{s}}\overline{\mathbf{T}}(s)^{-1}\overline{\mathbf{Q}}_{\mathbf{2}}(s)$; and $\overline{G}_d(s)=\overline{U}_d(s)/\overline{U}_{n2}(s)$.

According to equation (11), the control input signal for the NLSC shake table substructure test is determined from the transfer functions in equations (23) and (28). To simultaneously control the table acceleration and displacement, these signals need to be fed back to the control input signal. Then, the control input signal is described by the following equation:

$$u(s)=K_d''(s)\ddot{d}(s)+K_e(s)e(s)+K_\sigma''(s)\ddot{\sigma}(s), \tag{29}$$

where $e=y_{n2}-y_{ps}$; $\ddot{\sigma}\left(=\ddot{\sigma}_n-\ddot{\sigma}_p\right)=\left(\ddot{y}_{n2}-\ddot{\overline{y}}_{n2}\right)-\left(\ddot{y}_{ps}-\ddot{\overline{y}}_{ps}\right)$; and d is the acceleration of external disturbance d. Note that when the composite filter is employed, the error signal in equation (29) becomes $e=y_{n2}-y_{ps}^c$. By following equation (13), the controllers in equation (29) can be expressed as follows:

$$\begin{cases} K_d''(s)=\dfrac{\overline{U}_d(s)}{\left(\overline{U}_{n2}(s)+1\right)\overline{G}_{ps}(s)s^2}F_d(s), K_\sigma''(s)=\dfrac{1}{\left(\overline{U}_{n2}(s)+1\right)\overline{G}_{ps}(s)s^2}F_\sigma(s), K_e(s)=\dfrac{1}{\left(\overline{U}_{n2}(s)+1\right)\overline{G}_{ps}(s)}F_e(s). \end{cases} \tag{30}$$

By following the substructuring experiments with NLSC [53–56], this study employed $F_d(s) = 1$ and $F_e(s) = \omega_e^2/(s^2 + 2\omega_e s)$, where $\omega_e = 2\pi f_e$. In addition, $F_\sigma(s)$ was designed as a second-order Butterworth bandpass filter with a frequency range of 0.2–20 Hz. Hereafter, NLSC using these filters, including K_e based on the cut-off frequency f_e, is described as NLSC $\{K_e(f_e\,\text{Hz})\}$.

These filters affect stability, according to equation (16), and the design of the filters should be assessed from the stability viewpoint. Although these filters add some dynamics (e.g., phase lag) in the closed loops of NLSC, their influence is limited to its control performance when stability is maintained because of the nature of the DSS scheme, which is more robust against the delay than the HS scheme. Further details regarding the robustness of DSS can be found in the previous studies [42, 54].

3.2. Numerical Conditions. Two numerical examples were considered for the configuration shown in Figure 4. The emulate system in example 1 was designed by $m_{e1} = m_{e2} = m_{e3} = 200\,\text{kg}$, $c_{e1} = c_{e2} = c_{e3} = 120\,\text{Ns/m}$, and $k_{e1} = k_{e2} = k_{e3} = 43.0\,\text{kN/m}$, whereas the system in example 2 was $m_{e1} = m_{e2} = m_{e3} = 200\,\text{kg}$, $c_{e1}/2 = c_{e2}/1.5 = c_{e3} = 120\,\text{Ns/m}$, and $k_{e1}/2 = k_{e2}/1.5 = k_{e3} = 43.0\,\text{kN/m}$. Note that these parameters were determined from the actual parameters of the physical substructure in the experimental examination, as shown in Section 4.

Each storey of the emulate system has a nonlinear spring shown in Figure 5, and this nonlinear characteristic is described by

$$\begin{aligned} f_{eki}(t) = {} & r_{i2}k_{ei}\cdot\delta_i(t) + (1 - r_{i1})k_{ei}\cdot z_{i1}(t) \\ & + (r_{i1} - r_{i2})k_{ei}\cdot z_{i2}(t), \end{aligned} \tag{31}$$

where $\delta_i(t) = y_{ei}(t) - y_{ei-1}(t)$; $\dot{z}_{il}(t) = \dot{\delta}_i(t)\{\chi(\dot{\delta}_i(t))\chi(\Delta_{il} - z_{il}(t)) + \chi(-\dot{\delta}_i(t))\chi(\Delta_{il} + z_{il}(t))\}$ $(l = 1, 2)$; $\chi(a) = \{1\ (a \geq 0), 0\ (a < 0)\}$; Δ_{il} is the lth elastic limit of the spring on the ith storey; and r_{il} is the ith storey's reduction factor applied to the initial stiffness over the lth elastic limit. In the numerical examinations, the parameters of this nonlinear spring were fixed as $r_{11} = r_{21} = r_{31} = 0.5$, $r_{12} = r_{22} = r_{32} = 0.1$, $\Delta_{11} = \Delta_{21} = \Delta_{31}/2 = 0.015\,m$, and $\Delta_{12} = \Delta_{22} = \Delta_{32}/2 = 0.03\,m$, as shown in Figure 5. These properties are directly reflected in the corresponding substructures in shake table substructuring tests.

The substructuring tests in this study were performed using an earthquake acceleration record obtained by the Japan Meteorological Agency (JMA) during the 1995 Hyougo-ken Nanbu/Kobe earthquake. Its northwest component in Figure 6(a) is employed as the external disturbance of the experiments, and this component is referred to as the JMA Kobe motion in this study.

When the emulate systems for Examples 1 and 2 were directly excited by the JMA Kobe motion, they produced the responses in Figures 6(b) and 6(c), which are referred to as emulate responses in this study. In the emulate responses, the different conditions in Examples 1 and 2 caused a difference in the hysteresis on the 3rd storey, which remained within the elastic state in Example 1, whereas it went into the inelastic state in Example 2. In other words, Example 1 involves the inelasticity only in the numerical substructure, whereas Example 2 involves that in both numerical and physical substructures.

The emulate system for each example is divided into a numerical 2DOF substructure and an SDOF specimen placed on a shake table, and their parameters are $\{m_{n1}, m_{n2}, m_{p3}\} = \{m_{e1}, m_{e2}, m_{e3}\}$, $\{c_{n1}, c_{n2}, c_{p3}\} = \{c_{e1}, c_{e2}, c_{e3}\}$, and $\{k_{n1}, k_{n2}, k_{p3}\} = \{k_{e1}, k_{e2}, k_{e3}\}$. For both examples, a shake table is fixed to have the following parameters: $m_{ps} = 250\,\text{kg}$, $c_{ps} = 6.22\,\text{kN}\cdot\text{s/m}$ $k_{ps} = 103.6\,\text{kN/m}$ and $\tau = 0.004\,\text{s}$, which were decided from the actual physical substructure in Section 4. The nonlinear springs in the physical (numerical) substructure are described by equation (31) with their replacement of $f_{pki}(t)$, k_{pi}, and $\delta_i(t) = y_{pi}(t) - y_{pi-1}(t)$ ($f_{nki}(t)$, k_{ni}, and $\delta_i(t) = y_{ni}(t) - y_{ni-1}(t)$).

Linear models of the substructures were built by $\{\overline{m}_{n1}, \overline{m}_{n2}, \overline{m}_{p3}\} = \{m_{n1}, m_{n2}, m_{p3}\}$, $\{\overline{k}_{n1}, \overline{k}_{n2}, \overline{k}_{p3}\} = \{k_{n1}, k_{n2}, k_{p3}\}$, and $\{\overline{c}_{n1}, \overline{c}_{n2}, \overline{c}_{p3}\} = \{\gamma_c\cdot c_{n1}, \gamma_c\cdot c_{n2}, \gamma_c\cdot c_{p3}\}$, together with the linear model of the shake table: $\overline{m}_{ps} = m_{ps}$, $\overline{c}_{ps} = c_{ps}$, and $\overline{k}_{ps} = k_{ps}$. The highly damped linear model design can be activated by setting γ_c (>1) in the aforementioned damping elements.

3.3. Stability Robustness for Parameter Variations in Substructures. A series of stability analyses on NLSC is performed to examine the highly damped linear model design based on the numerical conditions of Examples 1 and 2, as well as the linear models designed in Section 3.1. Because the substructures in the examples have a nonlinear spring on each storey, the full consideration of the nonlinear characteristics in the stability analysis is an extremely difficult task. This is because the nonlinear characteristics change drastically depending on the deformation of the storeys, and this deformation is greatly affected by the external disturbance employed. Instead of considering all these factors, the stability here is analysed based on the equivalent models of substructures using the following parameters: $\{m_{n1}, m_{n2}, m_{p3}\}$, $\{c_{n1}, c_{n2}, c_{p3}\}$ and $\{\gamma_k k_{n1}, \gamma_k k_{n2}, \gamma_k k_{p3}\}$.

The analysis here equivalently considers the stiffness change in the nonlinear spring in Figure 5 by varying γ_k within the range 0.05–2.0 with increments of 0.05. Although the hysteretic loop of the spring has an energy-dissipation effect, which can be regarded as an additional damping effect [20], this study does not reflect this increase in its stability analysis. Thus, this analysis provides more conservative results than the actual stability of the substructuring tests.

In the stability analysis, the highly damped linear model design is handled as a variable γ_c (=1, 3, 5, and 10) which changes the damping terms of the linear model: $\{\overline{c}_{n1}, \overline{c}_{n2}, \overline{c}_{p3}\}$. In addition, the cut-off frequency f_e in $F_e(s)$ is also handled as a variable of $f_e = 1.0$, 3.0, and 10.0 Hz, to measure its influence on the stability. The stability of the NLSC for different sets of γ_k, γ_c, and f_e was analysed using the equivalent approach of the Nyquist stability criterion [56], and the results are summarised in Figures 7 and 8.

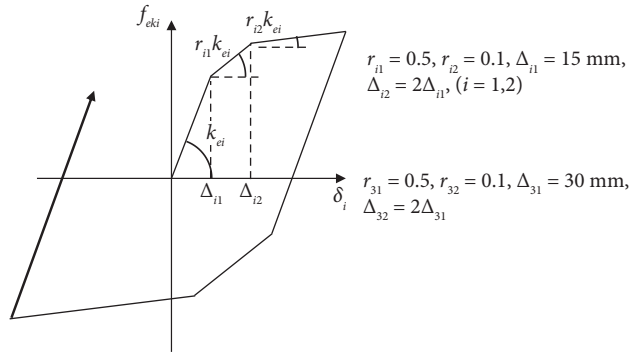

Figure 5: Nonlinear characteristics in emulate systems of Examples 1 and 2.

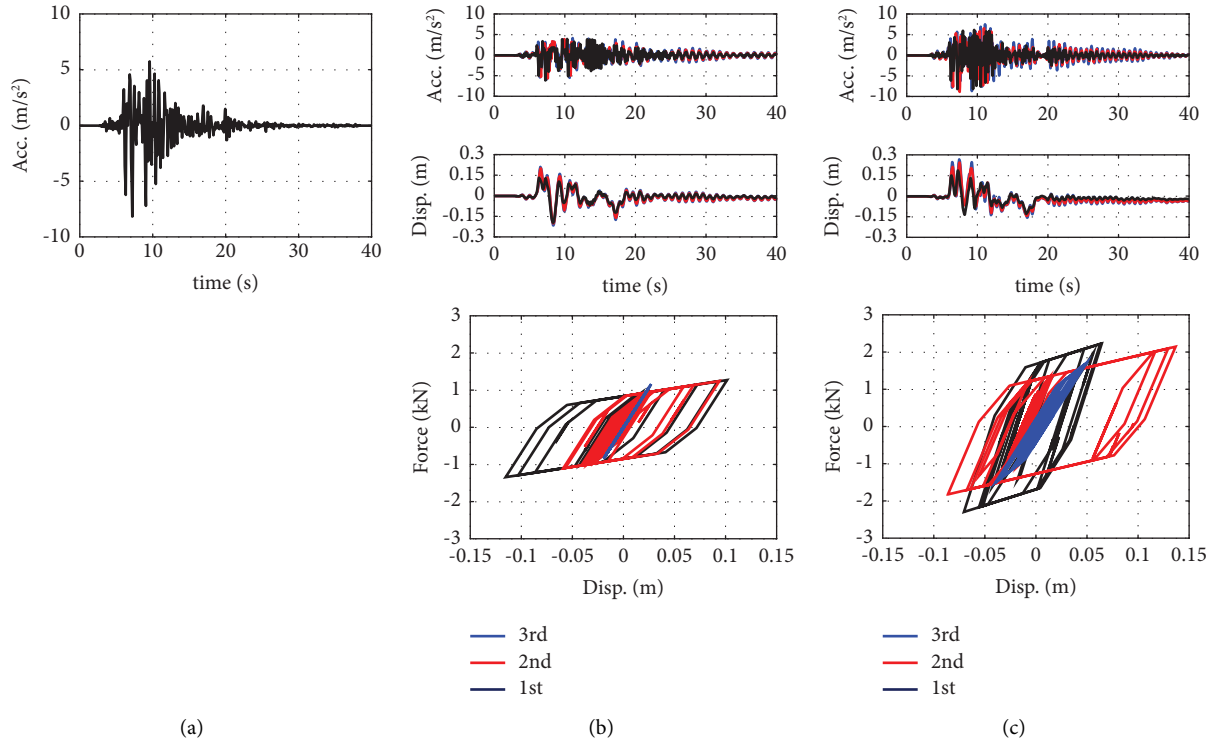

Figure 6: Responses of emulate systems under seismic excitations: (a) JMA Kobe motion, (b) emulate responses for Example 1, and (c) emulate responses for Example 2.

According to Figures 7 and 8, the highly damped linear model designs (i.e., $\gamma_c = 3, 5$ and 10) result in a wider stability range than the linear model using $\gamma_c = 1$. This study clarified the effectiveness of the design to enhance the robustness of NLSC against parameter variation. In addition, a higher cut-off frequency contributes to maintaining stability over a wider range of variations.

The nonlinear spring shown in Figure 5 becomes softer as the spring deformation increases. This indicates that the softening range of 0.05–1.0 is the prime information for stability analysis. In this range, NLSC $\{K_e(10\,\text{Hz})\}$ with linear models with $\gamma_c = 3, 5$, and 10 maintained stability for the wide range of variations, as shown in Figures 7(c) and 8(c), although instability was observed within a limited range. The narrow range of the instability may not be the critical issues in the implementation of NLSC shake table substructuring tests because this stability analysis does not consider the energy-dissipation derived from the nonlinear spring, resulting in more conservative results.

3.4. Numerical Examinations. To examine the proposed enhancements, numerical simulations were performed using shake table tests with NLSC $\{K_e(10\,\text{Hz})\}$ and linear models with $\gamma_c = 1, 3, 5$, and 10. The numerical results for Examples 1 and 2 are described in Sections 3.4.1 and 3.4.2, respectively. It should be noted that the linear model design with $\gamma_c = 1.0$ without the composite filter corresponds to the original NLSC, which does not use any enhancements and was employed in the first application of NLSC in shake table experiments [56].

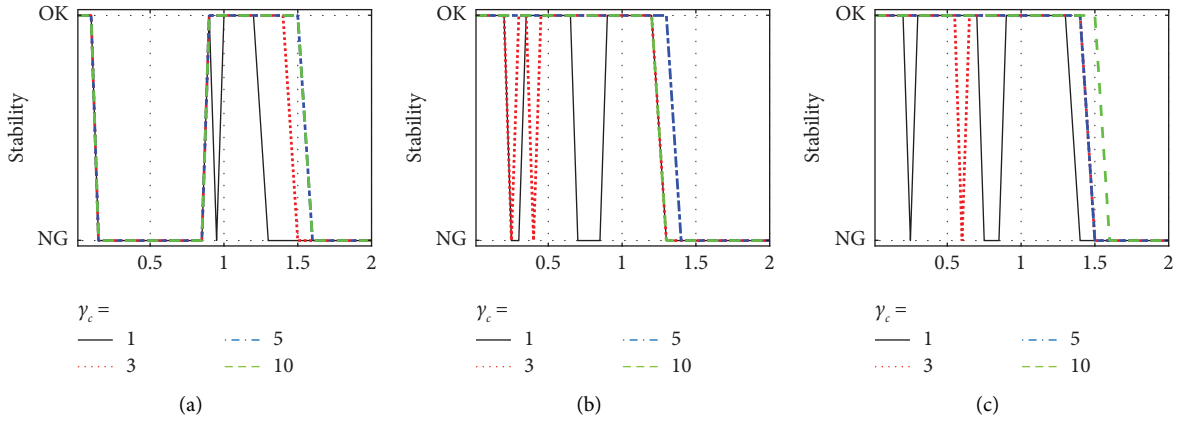

FIGURE 7: Stability analysis of NLSC $\{K_e(f_e\,\text{Hz})\}$ for example 1 with parameter variations: (a) $f_e = 1.0$ Hz, (b) $f_e = 3.0$ Hz, and (c) $f_e = 10.0$ Hz.

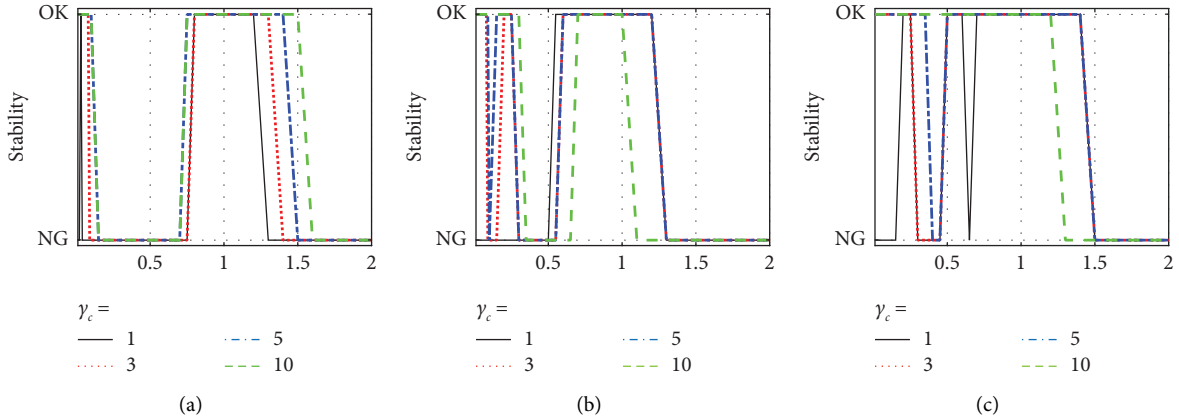

FIGURE 8: Stability analysis of NLSC $\{K_e(f_e\,\text{Hz})\}$ for Example 2 with parameter variations: (a) $f_e = 1.0$ Hz, (b) $f_e = 3.0$ Hz, and (c) $f_e = 10.0$ Hz.

For the examinations, this study employed the following indices to evaluate the accuracy of substructuring shake table tests in both the time and frequency domains:

$$S_t(y_0, y) = \frac{1}{1 + \sum (y_0(t) - y(t))^2 / \sum y_0(t)^2} \times 100\%,$$

$$S_f\left(A_{y0}, A_y\right) = \frac{1}{1 + \sum \left(A_{y0}(f) - A_y(f)\right)^2 / \sum A_{y0}(f)^2} \times 100\%, \tag{32}$$

where y is the signal to be compared by y_0; and $\{A_{y0}, A_y\}$ is the set of Fourier amplitude spectra of signals y_0 and y. This study focused on the frequency range 0.01–20.0 Hz for the evaluation of S_f.

Numerical examinations allow us to compare the results of the emulate responses and substructure responses in a substructuring test. Based on the displacement and acceleration of the table, the accuracy of the tests was evaluated by

$$\begin{cases} S_{fd}[e, pn] = \dfrac{S_f\left(A_{y_e}, A_{y_n}\right) + S_f\left(A_{y_e}, A_{y_p}\right)}{2}, \\ S_{td}[e, pn] = \dfrac{S_t(y_e, y_n) + S_t\left(y_e, y_p\right)}{2}, \\ S_{fa}[e, pn] = \dfrac{S_f\left(A_{\ddot{y}_e}, A_{\ddot{y}_n}\right) + S_f\left(A_{\ddot{y}_e}, A_{\ddot{y}_p}\right)}{2}, \\ S_{ta}[e, pn] = \dfrac{S_t(\ddot{y}_e, \ddot{y}_n) + S_t\left(\ddot{y}_e, \ddot{y}_p\right)}{2}, \\ S[e, pn] = \dfrac{S_{fa}[e, pn] + S_{td}[e, pn] + S_{fa}[e, pn] + S_{ta}[e, pn]}{4}. \end{cases} \tag{33}$$

Because emulated responses are not given to experimental examinations, their accuracy must be evaluated only by the responses of the substructures. Based on the table displacement and acceleration, the experimental examination was evaluated using the following indices:

$$\begin{cases} S_{fd}[n,p] = S_f\left(A_{y_n}, A_{y_p}\right),\ S_{td}[n,p] = S_t\left(y_n, y_p\right), \\ S_{fa}[n,p] = S_f\left(A_{\ddot{y}_n}, A_{\ddot{y}_p}\right),\ S_{ta}[n,p] = S_t\left(\ddot{y}_n, \ddot{y}_p\right), \\ S[n,p] = \dfrac{S_{fa}[n,p] + S_{td}[n,p] + S_{fa}[n,p] + S_{ta}[n,p]}{4}, \end{cases} \tag{34}$$

$S[e, pn]$ and $S[n, p]$ are the average values obtained from the other four indices in equations (33) and (34), respectively. The average value represents the overall accuracy of the shake table substructuring experiment.

3.4.1. Numerical Results for Example 1. Substructuring tests based on NLSC $\{K_e\,(10\,\text{Hz})\}$ were numerically simulated for example 1 with and without the highly damped linear model design, which is demonstrated with $\gamma_c = 1$, 3, 5, and 10, with and without a composite filter. The switching frequency of the composite filter in (18) was designed as $\omega_s = 1.0 \times 2\pi$. These simulations were performed by intentionally considering a set of noises in the table acceleration and displacement, and the noises were made such that they were not correlated with each other. Each noise is a series of random numbers processed by a second-order Butterworth filter with cut-off frequencies of 60.0 Hz. The noises for the table displacement and acceleration were adjusted to make the maximum values 2.0 mm and 0.1 m/s^2, respectively. Substructuring tests for the aforementioned conditions were performed using MATLAB/Simulink 2020a with a sampling time interval of 1.0 ms, and the obtained results are summarised in Table 1.

According to Table 1, the test of $\gamma_c = 1$ without the composite filter, which corresponds to the original NLSC, results in $S_{ta}[e, pn] = 45.9\%$ and $S_{ta}[n, p] = 22.5\%$. These low accuracies were derived from the noise amplification in the table acceleration, as shown in Figure 9(a). Other tests (i.e., $\gamma_c = 3$, 5, 10) without the composite filter also have similar results owing to the amplification, as shown in Table 1. The introduction of the composite filter was found to be effective in mitigating the noise amplification in the table acceleration, as clearly observed from the comparison between Figures 9(a) and 10(a). This result clarified that the noise amplification was caused by the feedback acting on the error signal that was directly obtained from the table displacement containing noise.

Regarding the control accuracy, the substructuring test with $\gamma_c = 1$ showed significant improvement by the introduction of the composite filter, resulting in $S_{ta}[e, pn] = 71.8\%$ and $S_{ta}[n, p] = 87.3\%$, although there is scope for further improvement. The highly damped linear model design with $\gamma_c = 3$ greatly improved the table acceleration accuracies, resulting in $S_{ta}[e, pn] = 91.2\%$ and $S_{ta}[n, p] = 96.3\%$ in Table 1. The increase in accuracy is owing to the improvement near 4.0 Hz, according to a comparison between Figures 10(a) and 11(a). The highly damped linear model design with $\gamma_c = 5$ produced results similar to those of $\gamma_c = 3$, as shown in Table 1. The test with $\gamma_c = 10$ resulted in lower similarities than those with $\gamma_c = 3$ and 5, indicating that excessively large damping coefficients impair the control performance.

The numerical examinations clarified the effectiveness of the two proposed enhancements, demonstrating that these enhancements can achieve accurate shake table substructuring tests that are not possible without them. It was also found that a highly damped linear model needs to be appropriately designed to not nullify the enhanced control performance.

3.4.2. Numerical Results for Example 2. Substructuring tests based on NLSC$\{K_e(10\,\text{Hz})\}$ were numerically simulated for example 2 with the identical conditions discussed in Section 3.4.1. Note that in these tests, the SDOF specimen on the table was expected to display some nonlinear characteristics according to the emulate responses of Example 2 in Figure 6(c). The results are summarised in Table 2.

The effectiveness of the composite filter is evident from the numerical results with and without the filter in Table 2. The composite filter significantly mitigated the noise amplification in the table acceleration, resulting in high accuracy in the frequency and time domains.

Although the substructuring test with $\gamma_c = 1$ and the composite filter achieved a sufficient accuracy of $S[e, pn] = 98.6\%$, the test with $\gamma_c = 3$ realised the best control in Figure 12, resulting in the highest accuracy of $S[e, pn] = 98.9\%$. The tests with $\gamma_c = 5$ and 10 resulted in lower accuracy than the test with $\gamma_c = 3$, indicating that extremely large additional damping given to the linear model eventually impairs the reliability of the experiments. This was observed in the case of Example 1 as well.

This examination has further validated the effectiveness of the two proposed enhancements and demonstrated the necessity of optimal additional damping in the linear model.

3.4.3. Numerical Results for Example 2A. The interaction between a specimen and the shake table is affected by the ratio of their masses. The mass ratios in Examples 1 and 2 were fixed, i.e., $m_{p3}/m_{ps} = 0.8$. To observe the control performance of NLSC for a different mass ratio, a set of additional numerical simulations was performed as Example 2A, in which the mass of the specimen was increased to 600 kg, and the other conditions were maintained identical to those of Example 2. The ratio in the case of Example 2A is $m_{p3}/m_{ps} = 2.4$. The numerical results of NLSC $\{K_e(10\,\text{Hz})\}$ using the composite filter and linear model design with $\gamma_c = 1, 3, 5$, and 10 are summarised in Table 3, and the result for $\gamma_c = 3$ is illustrated in Figure 13.

According to Table 3, NLSC $\{K_e\,(10\,\text{Hz})\}$ with $\gamma_c = 3$ exhibited the best control performance with $S\,[e, pn] = 98.2\%$. The accuracy of the table acceleration and

Table 1: Numerical results for Example 1.

	γ_c	S_{fd} [e, pn]	S_{td} [e, pn]	S_{fa} [e, pn]	S_{ta} [e, pn]	S [e, pn]	S_{fd} [n, p]	S_{td} [n, p]	S_{fa} [n, p]	S_{ta} [n, p]	S [n, p]
Without composite filter	1	99.4	98.5	78.0	45.9	80.4	99.9	99.5	95.3	22.5	79.3
	3	99.8	99.4	91.2	56.7	86.8	99.9	99.8	95.4	23.1	79.6
	5	99.8	99.7	91.4	57.1	87.0	99.95	99.8	95.8	23.2	79.7
	10	99.8	99.6	89.9	56.3	86.4	99.96	99.9	96.1	23.2	79.8
With composite filter	1	99.3	98.2	80.7	71.8	87.5	99.9	99.5	98.5	87.3	96.3
	3	99.7	99.3	94.7	91.2	96.2	99.9	99.8	99.4	96.3	98.9
	5	99.8	99.7	95.2	92.3	96.8	99.9	99.8	99.6	97.2	99.1
	10	99.8	99.7	93.6	90.8	96.0	99.96	99.9	99.7	97.4	99.2

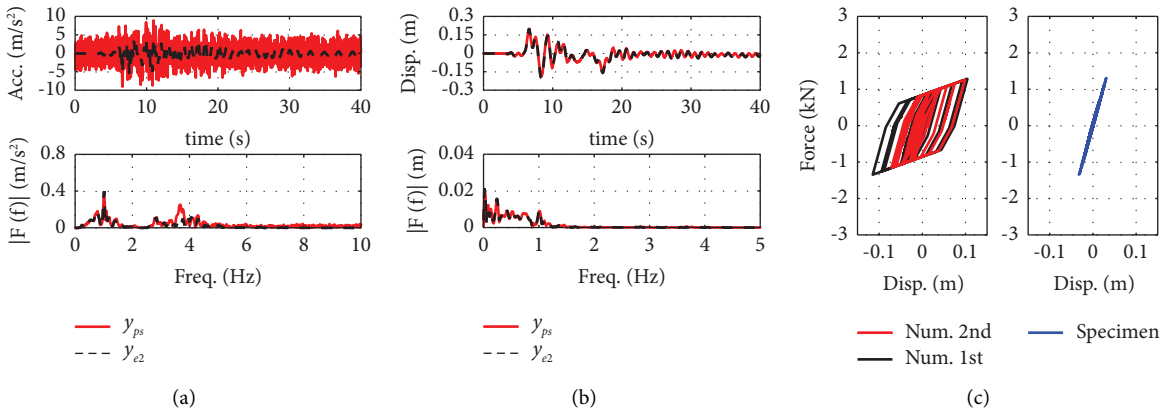

Figure 9: Numerical results of Example 1 with the original NLSC (i.e., $\gamma_c = 1$ without a composite filter): (a) table acceleration, (b) table displacement, and (c) hysteretic loops.

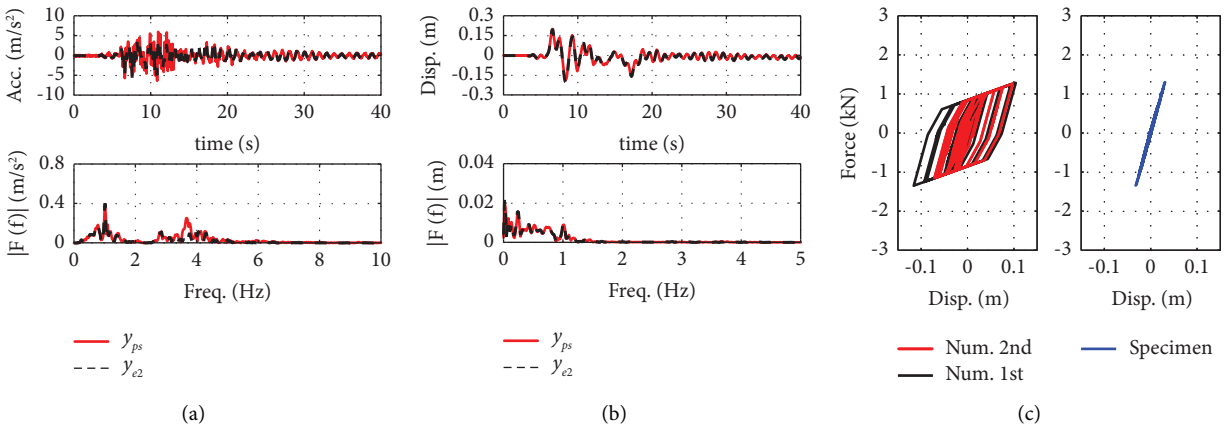

Figure 10: Numerical results of Example 1 with $\gamma_c = 1$ and a composite filter: (a) table acceleration, (b) table displacement, and (c) hysteretic loops.

displacement can be observed in Figures 13(a) and 13(b). It should be noted that the emulate response in the case of Example 2A shown in Fig. 13(a) differs from that in the case of Example 2 shown in Figure 12(a) because the mass increase in the specimen corresponds to the increasing relevant mass in the emulated system. As shown in Figure 13(c), the specimen for Example 2A displayed more severe nonlinearity than that for Example 2.

The results of Example 2A clarify the effectiveness of NLSC in shake table substructuring experiments that involve a specimen with severe nonlinear characteristics and significant interaction between the specimen and table.

4. Experimental Examination of NLSC

To examine the proposed enhancements, NLSC shake table substructuring experiments were performed using a single-axis electrodynamic shake table and an SDOF specimen, as shown in Figure 14(a). The specimen and shake table

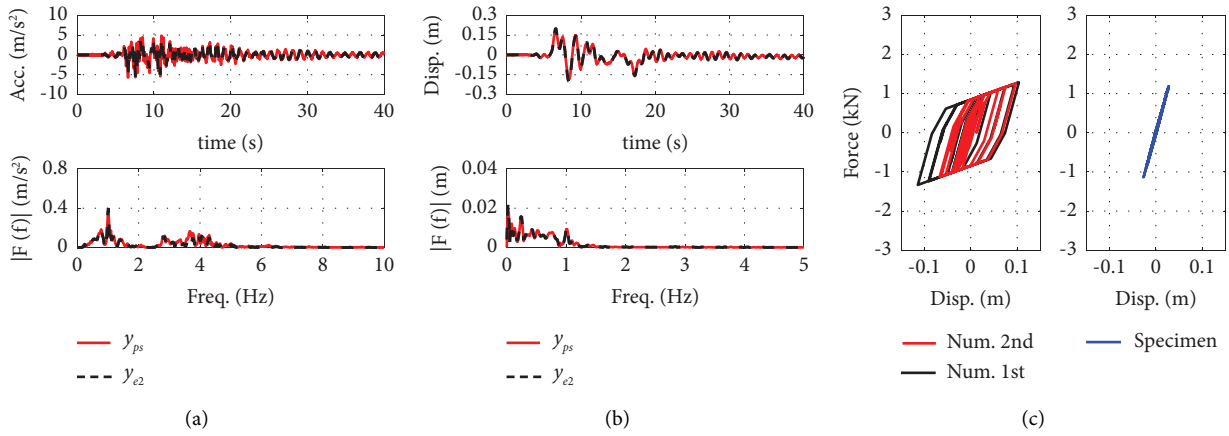

Figure 11: Numerical results of Example 1 with $\gamma_c = 3$ and a composite filter: (a) table acceleration, (b) table displacement, and (c) hysteretic loops.

Table 2: Numerical results for Example 2.

	γ_c	S_{fd} $[e, pn]$	S_{td} $[e, pn]$	S_{fa} $[e, pn]$	S_{ta} $[e, pn]$	S $[e, pn]$	S_{fd} $[n, p]$	S_{td} $[n, p]$	S_{fa} $[n, p]$	S_{ta} $[n, p]$	S $[n, p]$
Without composite filter	1	99.96	99.8	96.9	67.1	91.0	99.97	99.9	97.1	37.7	83.7
	3	99.9	99.8	97.2	67.3	91.1	99.98	99.9	97.6	37.9	83.8
	5	99.9	99.8	96.5	66.8	90.7	99.98	99.9	97.8	37.9	83.9
	10	99.9	99.8	93.2	63.0	89.0	99.98	99.9	98.1	37.9	84.0
With composite filter	1	99.96	99.9	98.3	96.2	98.6	99.97	99.9	99.0	96.9	99.0
	3	99.95	99.8	98.7	97.0	98.9	99.98	99.9	99.5	97.9	99.3
	5	99.9	99.8	98.0	96.2	98.5	99.98	99.9	99.6	98.0	99.4
	10	99.9	99.9	94.6	90.2	96.1	99.98	99.9	99.7	97.4	99.3

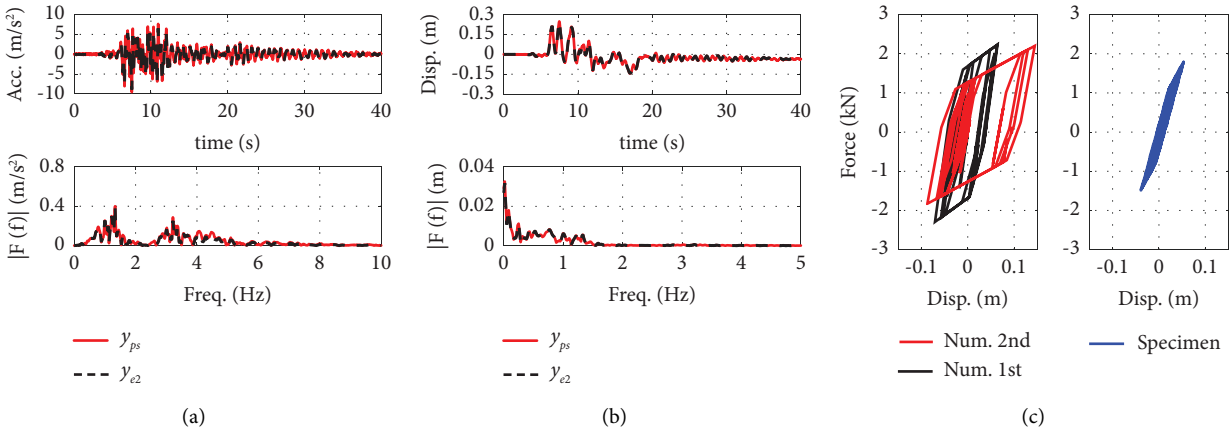

Figure 12: Numerical results of Example 2 with $\gamma_c = 3.0$ and a composite filter: (a) table acceleration, (b) table displacement, and (c) hysteretic loops.

combined were handled as the physical substructure for the substructuring experiments in this study.

This shake table has the following specifications: the table size is 1.2×1.2 m with a weight of 200 kg, the maximum stroke is ±0.3 m, the maximum acceleration is 19.8 (9.8) m/s^2 under the loading condition of 150 (500) kg, and the maximum velocity is 1.4 m/s. As the set of experimental rigs directly placed on the table weighed 50 kg, the table mass became $m_{ps} = 250$ kg. The weight of the specimen's steel mass was measured to be $m_{p3} = 200$ kg. The steel mass was connected to the table via steel plates, demonstrating the flexibility of the specimen. The plates were expected to display nonlinear characteristics owing to their yielding when the deformation exceeded its elastic limit.

The shake table was equipped with a magnetostrictive displacement transducer and two servo accelerometers for

Table 3: Numerical results for Example 2A.

	γ_c	S_{fd} [e, pn]	S_{td} [e, pn]	S_{fa} [e, pn]	S_{ta} [e, pn]	S [e, pn]	S_{fd} [n, p]	S_{td} [n, p]	S_{fa} [n, p]	S_{ta} [n, p]	S [n, p]
	1	99.8	98.5	98.2	95.8	98.1	99.9	99.9	99.2	97.4	99.1
With	3	99.8	98.9	98.1	96.0	98.2	99.96	99.9	99.6	98.2	99.4
composite filter	5	99.8	98.9	96.3	93.5	97.1	99.96	99.9	99.7	98.3	99.5
	10	99.6	98.4	83.3	79.1	90.1	99.96	99.9	99.8	97.7	99.4

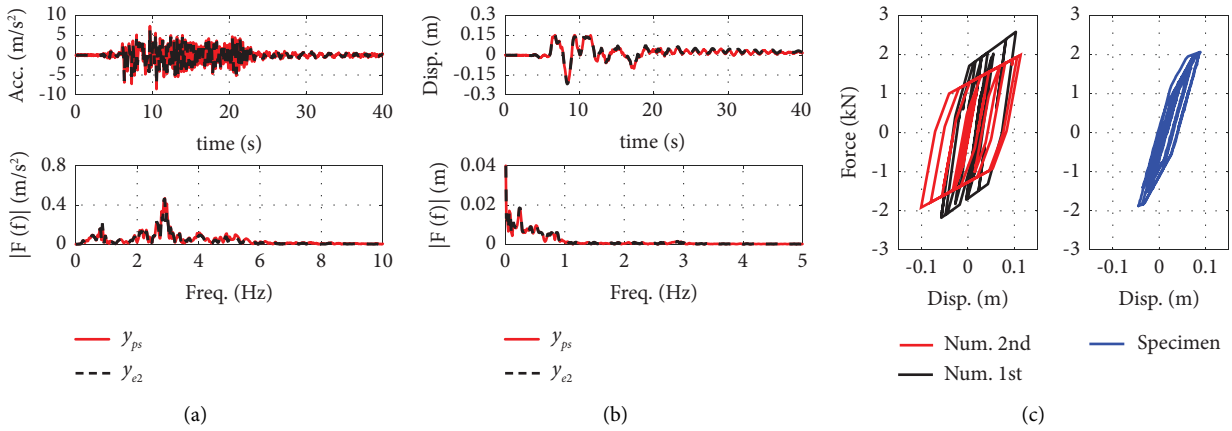

Figure 13: Numerical results of Example 2A with $\gamma_c = 3.0$ and a composite filter: (a) table acceleration, (b) table displacement, and (c) hysteretic loops.

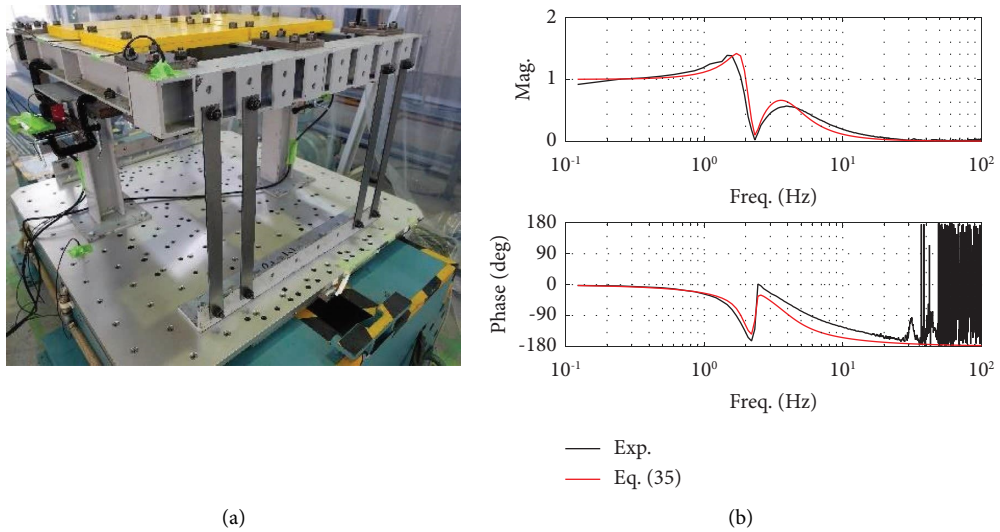

Figure 14: Physical substructures including a single-axis shake table: (a) experimental setup and (b) table dynamics obtained by a system identification test.

control. To measure the responses of the specimen, two wire displacement transducers were placed between the table and steel mass, and two strain gauge accelerometers were placed on the mass.

Prior to the experiments, the dynamics of the physical substructures were investigated via system identification, and the details are described in Section 4.1. Based on this identification, NLSC shake table substructuring experiments were performed, and the results are shown in Section 4.2.

4.1. Experimental Conditions. System identification was performed to investigate the dynamics of the shake table sustaining the SDOF specimen using band-limited white noise. This white noise was used as the reference displacement signal to be realised in the table, and its maximum amplitude was adjusted to no greater than 15.0 mm.

In the system identification, the pure time delay in this shake table system was found to be $\tau = 0.004$ s. The pure time delay is believed to be derived from the shake table systems (e.g., AD/DA converters or the digital signal processor) or

caused by some unmodelled higher dynamics of the table that cannot be modelled by the mass-spring-damper model employed in this study. The identified transfer function is illustrated in Figure 14(b). Furthermore, based on the same form of equation (23), it has been reasonably modelled using the following equation:

$$G_{ps}(s)\left(=\frac{y_{ps}(s)}{u(s)}\right) = \frac{414.5s^2 + 248.7s + 8.913e04}{s^4 + 25.96s^3 + 816.5s^2 + 5598s + 8.913e04}. \quad (35)$$

Based on the known masses (m_{ps} and m_{p3}) and equation (23), the shake table and specimen were found to have the following properties: $c_{ps} = 6220$ Ns/m; $k_{ps} = 103.6$ kN/m; $m_{p3} = 200$ kg; $c_{p3} = 120$ Ns/m; and $k_{p3} = 43.0$ kN/m.

Based on the identified properties, the linear model $\overline{G}_{ps}(s)$ used in NLSC is built using equation (23) with the following setting: $\overline{m}_{ps} = m_{ps}, \overline{c}_{ps} = c_{ps}, \overline{k}_{ps} = k_{ps}$, $\{\overline{m}_{n1}, \overline{m}_{n2}, \overline{m}_{p3}\} = \{m_{n1}, m_{n2}, m_{p3}\}$, $\{\overline{k}_{n1}, \overline{k}_{n2}, \overline{k}_{p3}\} = \{k_{n1}, k_{n2}, k_{p3}\}$, and $\{\overline{c}_{n1}, \overline{c}_{n2}, \overline{c}_{p3}\} = \{\gamma_c c_{n1}, \gamma_c c_{n2}, \gamma_c c_{p3}\}$, which is tuned by γ_c for the highly damped linear model design. In the case of $\gamma_c = 1$, the linear model becomes identical to equation (35). The estimate of the pure time delay was assumed to be $\overline{\tau} = 0.004$s, according to the identification result.

4.2. Experimental Examinations. Shake table substructuring experiments based on NLSC $\{K_e$ (10 Hz)$\}$ were performed for the configuration shown in Figure 15 with the JMA Kobe motion and the conditions of Examples 1 and 2 as well as the nonlinear characteristics shown in Figure 5. These experiments were performed using dSPACE (MicroLabBox) and MATLAB/Simulink 2020a with a time sampling interval of 1.0 ms.

To examine the enhancements (i.e., composite filtering technique and highly damped linear model design), actual substructuring experiments were executed for Example 1 with NLSC with the linear model design of $\gamma_c = 1$ and 3 with and without the composite filter. It should be noted that the linear model design of $\gamma_c = 1$ without the composite filter corresponds to the original NLSC, which does not have any enhancements. In these experiments, the amplitude of the JMA Kobe motion was scaled down to 15%. The experimental results are shown in Figure 16. As anticipated from the numerical examination, a shake table substructuring experiment without the composite filter resulted in noise amplification, as shown in Figure 16(a). This experiment was manually terminated at approximately 5.0 s for safety reasons. By contrast, the experiment with the composite filter did not produce such a large noisy acceleration, as shown in Figure 16(b).

This comparison verified the effectiveness of the composite filter. Thus, the following substructuring experiments for 100% amplitude were performed only with the composite filter.

4.2.1. Experimental Results for Example 1. NLSC substructuring experiments for Example 1 were performed with the composite filter and highly damped linear model design using $\gamma_c = 1$ and 3, although the designs with $\gamma_c = 5$ and 10 were not performed because excessively large damping coefficients impaired the control performance in the numerical simulations, as shown in Table 1. It should be noted that each experiment was performed using new steel plates in the specimens. The experimental results without post-processing are illustrated in Figures 17 and 18, and the indices obtained using equation (34) are listed in Table 4.

The experiment with $\gamma_c = 1$ achieved simultaneous control of table acceleration and displacement with reasonable accuracy, as shown in Figure 17. $S_{ta}[n, p]$ in Table 4 is not as high as the other indices, and this tendency corresponds to the simulation of $\gamma_c = 1$ in Table 1. The experiment with $\gamma_c = 3$ achieved simultaneous control with higher accuracies than the experiment with $\gamma_c = 1$, as shown in Figure 18 and Table 4. The highly damped linear model design with $\gamma_c = 3$ resulted in $S_{ta}[n, p] = 96.3\%$, which is better than $S_{ta}[n, p] = 89.8\%$ in the design with $\gamma_c = 1$, clarifying the effectiveness of the design.

In the actual implementation of a substructuring experiment, its reliability cannot be assessed by comparison with an emulate response because of its absence. In general, an experiment with higher similarities between substructure responses is more reliable than an experiment with lower similarities. In this regard, the experiment with $\gamma_c = 3$ is believed to be sufficiently reliable, because all indices obtained from both substructures' responses are no smaller than 96%.

At the first application of NLSC to a shake table [56], the experiment on Example 1 with 100% JMA Kobe was impossible because of the noise amplification issue and insufficient robustness against parameter variations in the substructures. The enhancements proposed in this study resulted in an experiment with high accuracy.

4.2.2. Experimental Results for Example 2. NLSC substructuring experiments for Example 2 were performed with the composite filter and highly damped linear model design using $\gamma_c = 1$ and 3, although the designs with $\gamma_c = 5$ and 10 were not performed because of the same reason mentioned in Section 4.2.1. The experimental results without post-processing are illustrated in Figures 19 and 20, and the indices obtained using equation (34) are listed in Table 5. Note that these experiments were also performed by replacing the steel plates with new plates in each experiment.

According to Table 5, the experiment with $\gamma_c = 1$ resulted in $S_{ta}[n, p] = 73.5\%$ which was not satisfactory. This low accuracy was due to the undesired high-frequency component observed at over 35 s, as shown in Figure 19(a). The postcondition of the SDOF specimen after experiencing the severe nonlinear characteristics in Figure 19(c) presumably changed the overall dynamics of the physical substructure, causing the generation of the undesired component.

The experiment with $\gamma_c = 3$ achieved accurate simultaneous control of the table acceleration and displacement, as shown in Figures 20(a) and 20(b), despite the severe nonlinear characteristics of the SDOF specimen in Figure 20(c). In addition, all accuracies in this experiment have become

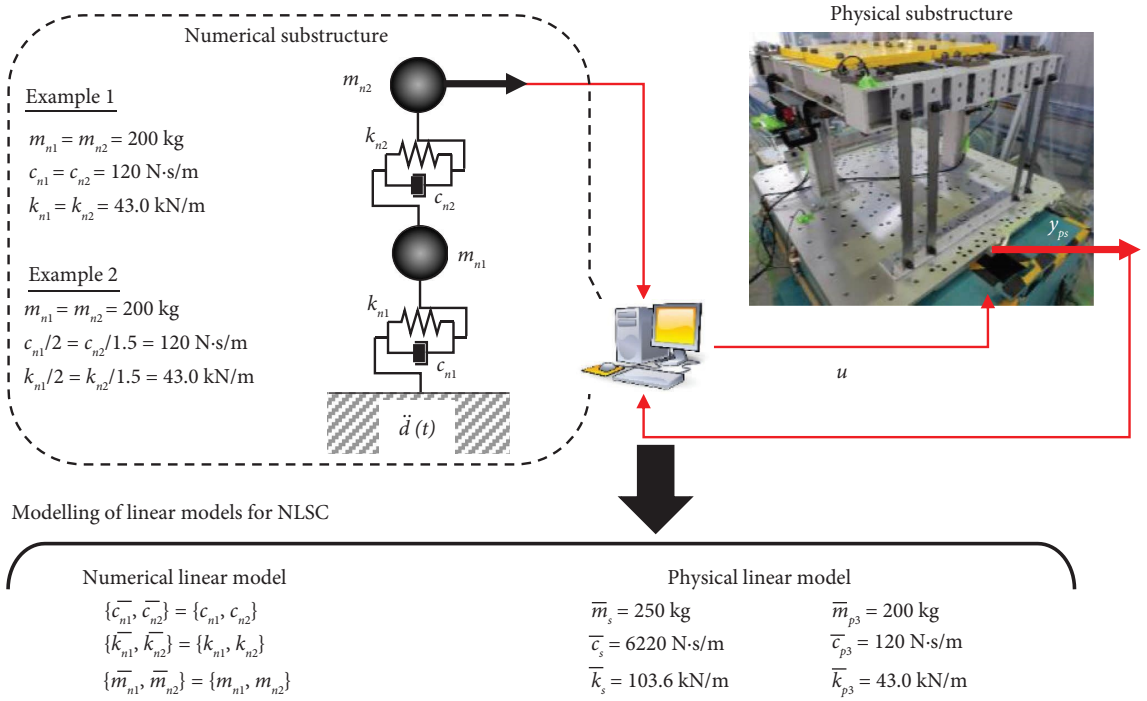

Figure 15: Configuration of shake table substructuring experiments.

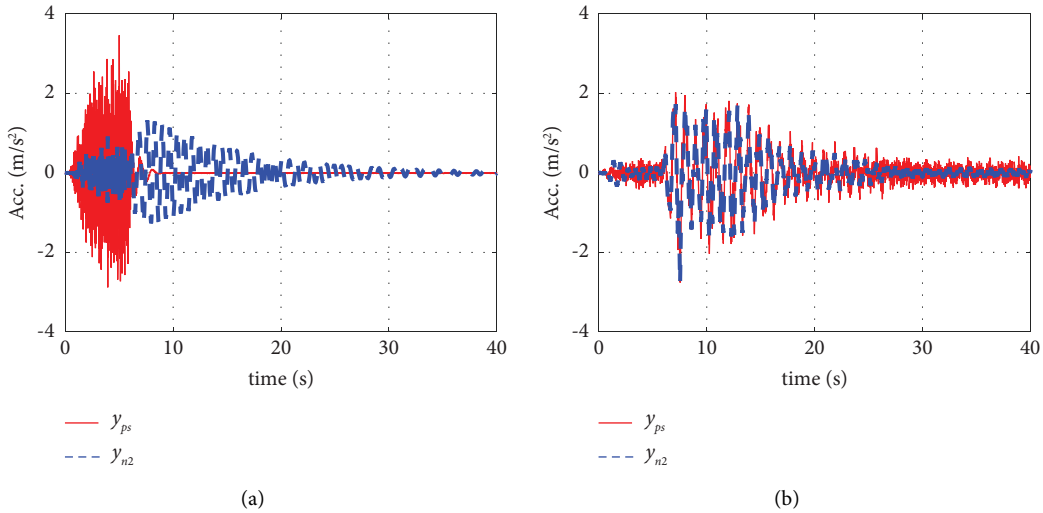

Figure 16: Table accelerations for Example 1 with 15% JMA Kobe motion: (a) NLSC $\{K_e$ (10 Hz)$\}$ without the composite filter (i.e., the original NLSC) and (b) NLSC $\{K_e$ (10 Hz)$\}$ with the composite filter.

sufficiently high in Table 5 because of the highly damped linear model, which prevented the occurrence of the undesired high-frequency component generated in the experiment with $\gamma_c = 1$ in Figure 19(a).

According to the aforementioned comparison, a highly damped linear model design is essential to perform a reliable shake table substructuring experiment involving nonlinear characteristics with high accuracy.

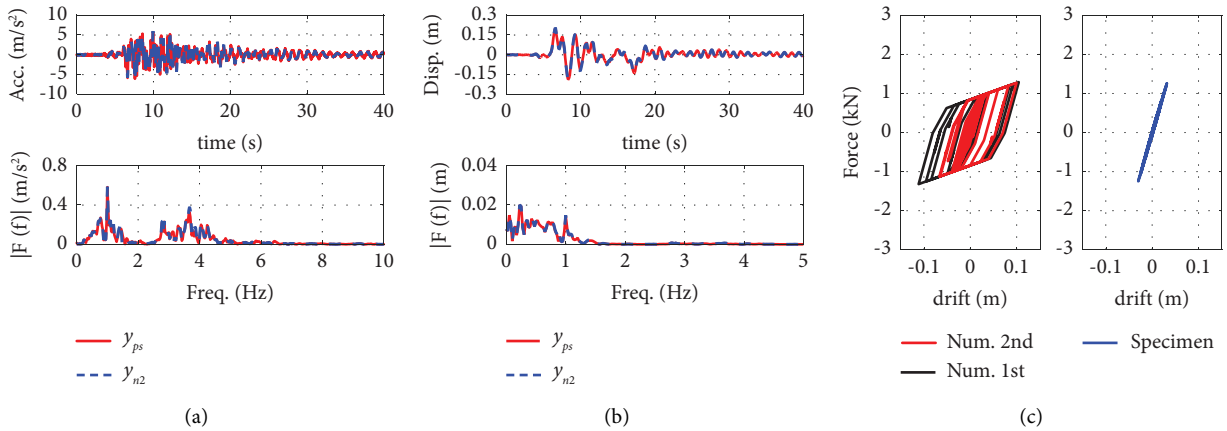

Figure 17: Experimental results of Example 1 with γ_c = 1.0: (a) table acceleration, (b) table displacement, and (c) hysteretic loops.

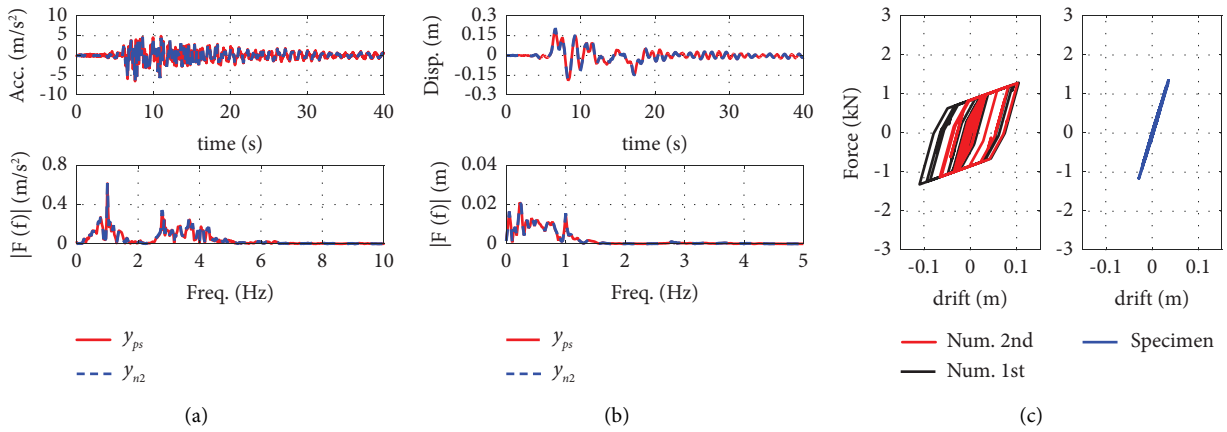

Figure 18: Experimental results of Example 1 with γ_c = 3.0: (a) table acceleration, (b) table displacement, and (c) hysteretic loops.

Table 4: Experimental results for Example 1 with γ_c = 1 and 3.

	γ_c	S_{fd} [n, p]	S_{td} [n, p]	S_{fa} [n, p]	S_{ta} [n, p]	S [n, p]
With composite filter	1	99.9	99.2	98.4	89.8	96.8
	3	99.9	99.7	99.3	96.3	98.8

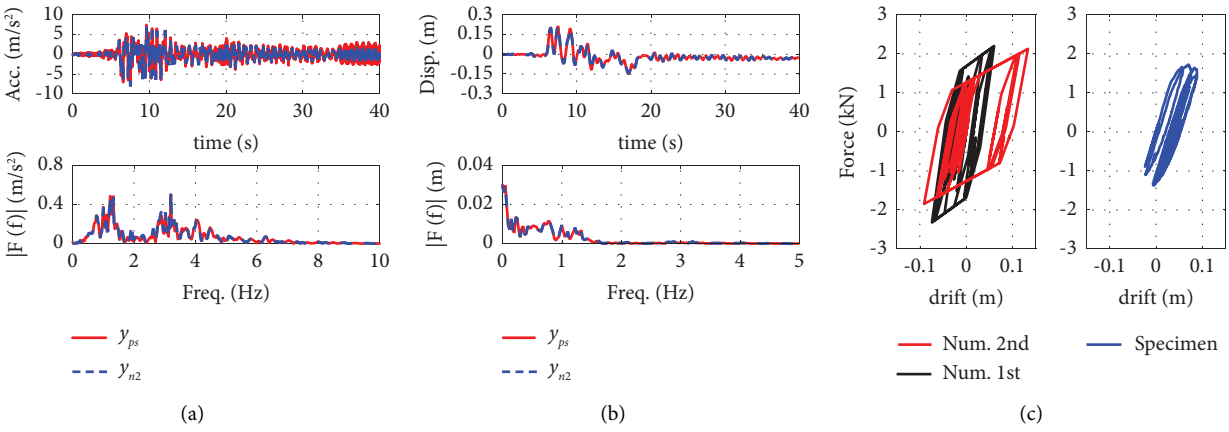

Figure 19: Experimental results of Example 2 with γ_c = 1: (a) table acceleration, (b) table displacement, and (c) hysteretic loops.

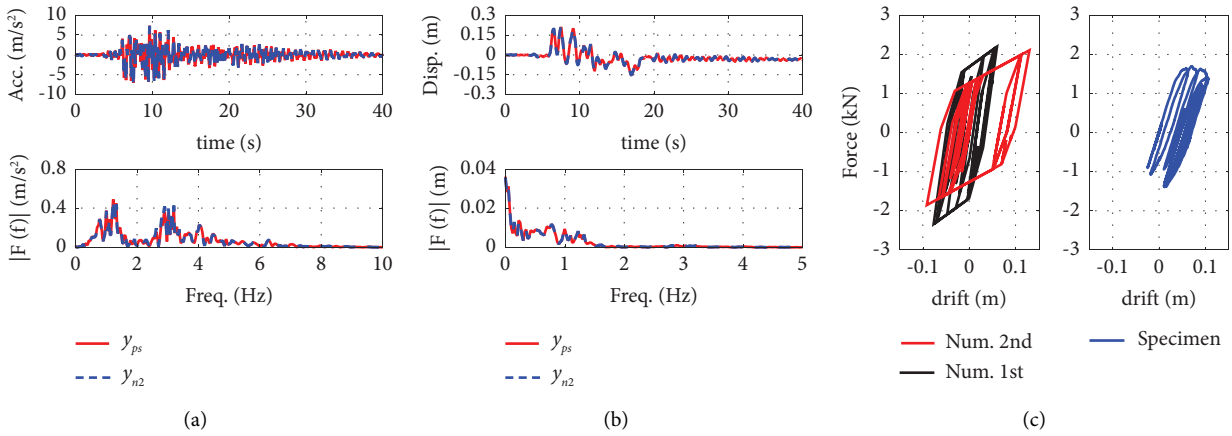

Figure 20: Experimental results of Example 2 with $\gamma_c = 3$: (a) table acceleration, (b) table displacement, and (c) hysteretic loops.

Table 5: Experimental results for Example 2 with $\gamma_c = 1$ and 3.

	γ_c	S_{fd} $[n, p]$	S_{td} $[n, p]$	S_{fa} $[n, p]$	S_{ta} $[n, p]$	S $[n, p]$
With composite filter	1	99.9	99.8	98.5	73.5	92.9
	3	99.97	99.9	99.3	97.2	99.1

5. Conclusions

This study introduced two techniques to enhance the NLSC for shake table substructuring experiments involving severe nonlinear characteristics. One is a composite filtering technique to minimise noise contaminating displacement data, and the other is a highly damped linear model design to enhance the robustness of NLSC against nonlinear characteristics. The detailed conclusions of this study are summarised as follows.

(i) The error feedback action in NLSC requires a controller designed with a high cut-off frequency to enhance its robustness against nonlinear characteristics. However, a controller with a higher cut-off frequency resulted in more significant noise amplification in the table acceleration. To minimise noise amplification, the displacement data fed back to the error feedback action must be reduced maximally. For this reduction, this study employed the composite filtering technique, which is the data fusion of the table acceleration and displacement. In addition, this study introduced a highly damped linear model design to further enhance the robustness of NLSCs against nonlinear characteristics. In this design, a model with a larger damping than an actual controlled system is built for NLSC, which can handle the modelling gap as a type of nonlinear characteristic.

(ii) For numerical examinations, NLSC shake table substructuring tests with enhancements were simulated for two examples using a numerical 2DOF substructure and a physical substructure with the JMA Kobe motion. In the stability analyses for examples 1 and 2, the robustness of NLSC against parameter variations was enhanced by the highly damped linear model design and the error feedback action with a high cut-off frequency. This enhanced robustness was attained at the slight expense of the table control accuracy, and an unreasonably high damped design may result in a significant loss of the accuracy. In the numerical examinations, the composite filtering technique clearly reduced the noise in the displacement data and minimised the noise amplification in the acceleration of the table. This noise reduction allowed us to design an error feedback controller with a high cut-off frequency, which is key to enhancing the robustness of NLSC against parameter variations. In the examination, NLSC with the two enhancements achieved accurate shake table substructuring tests with the full amplitude of the JMA Kobe motion along with severe nonlinear characteristics in the substructures.

(iii) Experimental examinations were performed for an actual physical substructure consisting of a shake table and an SDOF specimen under identical conditions (Examples 1 and 2) used in the numerical examinations and the full amplitude of the JMA Kobe motion. During the examinations, NLSC with the enhancements achieved shake table substructuring experiments with high accuracies of over 96% despite the substructures displaying severe nonlinear characteristics owing to large deformations. These experiments were not possible without the enhancements proposed in this study, and their effectiveness was clarified in this study.

This study clarified the effectiveness of NLSC shake table substructuring experiments with enhancements for a 3DOF structure with severe nonlinear characteristics. To examine

its feasibility for more complicated structures, it will be applied to a higher-order system that demonstrates a higher building. In addition, the current stability analysis is limited as an approximate guide for investigating the stability of NLSC shake table substructuring experiments involving nonlinear characteristics. The stability analysis needs to be further elaborated so that it can more precisely evaluate the stability of shake table substructuring experiments with nonlinear characteristics. The linear model design for NLSC can be further elaborated to systematically determine its optimal parameters.

Data Availability

The data used to support the findings of this study are available from the corresponding author upon request.

Conflicts of Interest

The authors declare that they have no conflicts of interest.

Acknowledgments

This study was supported by the research grants (Nos. 20H02228 and 22K18838) from the Japan Society for the Promotion of Science.

References

[1] R. T. Severn, "The development of shaking tables-A historical note," *Earthquake Engineering & Structural Dynamics*, vol. 40, no. 2, pp. 195–213, 2011.

[2] T. Horiuchi, M. Inoue, T. Konno, and W. Yamagishi, "Development of a real-time hybrid experimental system using a shaking table. (Proposal of experiment concept and feasibility study with rigid secondary system)," *JSME Int J Ser C*, vol. 42, no. 2, pp. 255–264, 1999.

[3] S. A. Neild, D. P. Stoten, D. Drury, and D. J. Wagg, "Control issues relating to real-time substructuring experiments using a shaking table," *Earthquake Engineering & Structural Dynamics*, vol. 34, no. 9, pp. 1171–1192, 2005.

[4] M. Nakashima, T. Nagae, R. Enokida, and K. Kajiwara, "Experiences, accomplishments, lessons, and challenges of E-defense – Tests using world's largest shaking table," *Jpn Archit Rev*, vol. 1, no. 1, pp. 4–17, 2018.

[5] Y. Tagawa and K. Kajiwara, "Controller development for the E-Defense shaking table," *Proceedings of the Institution of Mechanical Engineers - Part I: Journal of Systems & Control Engineering*, vol. 221, no. 2, pp. 171–181, 2007.

[6] K. P. Ryu and A. M. Reinhorn, "Real-time control of shake tables for nonlinear hysteretic systems," *Structural Control and Health Monitoring*, vol. 24, no. 2, Article ID e1871, 2017.

[7] J. Yao, M. Dietz, R. Xiao, H. Yu, T. Wang, and D. Yue, "An overview of control schemes for hydraulic shaking tables," *Journal of Vibration and Control*, vol. 22, no. 12, pp. 2807–2823, 2016.

[8] R. Enokida and K. Kajiwara, "Nonlinear signal-based control for single-axis shake tables supporting nonlinear structural systems," *Structural Control and Health Monitoring*, vol. 26, no. 9, Article ID e2376, 2019.

[9] D. Stoten and E. Gómez, "Adaptive control of shaking tables using the minimal control synthesis algorithm," *Philosophical Transactions of the Royal Society of London,Series A: Mathematical, Physical and Engineering Sciences*, vol. 359, no. 1786, pp. 1697–1723, 2001.

[10] D. Stoten and N. Shimizu, "The feedforward minimal control synthesis algorithm and its application to the control of shaking-tables," *Proceedings of the Institution of Mechanical Engineers - Part I: Journal of Systems & Control Engineering*, vol. 221, no. 3, pp. 423–444, 2007.

[11] A. Gizatullin and K. Edge, "Adaptive control for a multi-axis hydraulic test rig," *Proceedings of the Institution of Mechanical Engineers - Part I: Journal of Systems & Control Engineering*, vol. 221, no. 2, pp. 183–198, 2007.

[12] Y. Landau, *Adaptive Control: The Model Reference Approach*, Dekker, New York, NY, USA, 1979.

[13] B. Phillips, N. Wierschem, and B. Spencer Jr, "Model-based multi-metric control of uniaxial shake tables," *Earthquake Engineering & Structural Dynamics*, vol. 43, no. 5, pp. 681–699, 2014.

[14] A. Plummer, "Model-based motion control for multi-axis servohydraulic shaking tables," *Control Engineering Practice*, vol. 53, pp. 109–122, 2016.

[15] A. Najafi and B. F. Spencer, "Modified model-based control of shake tables for online acceleration tracking," *Earthquake Engineering & Structural Dynamics*, vol. 49, no. 15, pp. 1721–1737, 2020.

[16] A. Maekawa, C. Yasuda, and T. Yamashita, "Application of H∫ infin; control to a 3-D shaking table," *Transactions of the Society of Instrument and Control Engineers*, vol. 29, no. 9, pp. 1094–1103, 1993.

[17] P. C. Chen, C. T. Lai, and K. C. Tsai, "A control framework for uniaxial shaking tables considering tracking performance and system robustness," *Structural Control and Health Monitoring*, vol. 24, no. 11, Article ID e2015, 2017.

[18] R. Enokida, I. Takewaki, and D. Stoten, "A nonlinear signal-based control method and its applications to input identification for nonlinear SIMO problems," *Journal of Sound and Vibration*, vol. 333, no. 24, pp. 6607–6622, 2014.

[19] R. Enokida, "Stability of nonlinear signal-based control for nonlinear structural systems with a pure time delay," *Structural Control and Health Monitoring*, vol. 26, no. 8, Article ID e2365, 2019.

[20] R. Enokida and K. Kajiwara, "Simple piecewise linearisation in time series for time-domain inversion to estimate physical parameters of nonlinear structures," *Structural Control and Health Monitoring*, vol. 27, no. 10, pp. 1–23, 2020.

[21] R. Enokida, K. Ikago, J. Guo, and K. Kajiwara, "Nonlinear signal-based control for shake table experiments with sliding masses," *Earthquake Engineering & Structural Dynamics*, vol. 52, no. 6, pp. 1908–1931, 2023.

[22] R. Enokida, K. Ikago, and K. Kajiwara, "Numerically disturbed shake table experimentation to examine nonlinear signal-based control," *Front Built Environ*, vol. 8, pp. 1–14, 2022.

[23] R. Enokida, "Enhancement of nonlinear signal-based control to estimate earthquake excitations from absolute acceleration responses of nonlinear structures," *Mechanical Systems and Signal Processing*, vol. 181, Article ID 109486, 2022.

[24] S. K. Lee, E. C. Park, K. W. Min, and J. H. Park, "Real-time substructuring technique for the shaking table test of upper substructures," *Engineering Structures*, vol. 29, no. 9, pp. 2219–2232, 2007.

[25] R. Zhang, B. M. Phillips, S. Taniguchi, M. Ikenaga, and K. Ikago, "Shake table real-time hybrid simulation techniques for the performance evaluation of buildings with inter-story isolation," *Structural Control and Health Monitoring*, vol. 24, no. 10, pp. 1–19, 2017.

[26] A. H. Schellenberg, T. C. Becker, and S. A. Mahin, "Hybrid shake table testing method: theory, implementation and application to midlevel isolation," *Structural Control and Health Monitoring*, vol. 24, no. 5, pp. 1–18, 2017.

[27] S. Y. Chu, L. Y. Lu, and S. W. Yeh, "Real-time hybrid testing of a structure with a piezoelectric friction controllable mass damper by using a shake table," *Structural Control and Health Monitoring*, vol. 25, no. 3, p. e2124, 2018.

[28] S. Yoshida, H. Fujitani, Y. Mukai, and M. Ito, "Real-time hybrid simulation of semi-active control using shaking table: proposal and verification of a testing method for mid-story isolated buildings," *Jpn Archit Rev*, vol. 1, no. 2, pp. 221–234, 2018.

[29] Z. Tang, M. Dietz, Y. Hong, and Z. Li, "Performance extension of shaking table-based real-time dynamic hybrid testing through full state control via simulation," *Structural Control and Health Monitoring*, vol. 27, no. 10, pp. 1–19, 2020.

[30] M. Hakuno, M. Shidawara, and T. Hara, "Dynamic destructive test of a cantilever beam, controlled by an analog-computer," *Proceedings of the Japan Society for Comparative Endocrinology*, vol. 1969, no. 171, pp. 1–9, 1969.

[31] K. Takanashi, K. Udagawa, M. Seki, T. Okada, and H. Tanaka, "Non-linear earthquake response analysis of structures by a computer-actuator on-line system: part 1 detail of the system," *Transactions of the Architectural Institute of Japan*, vol. 229, no. 0, pp. 77–83, 1975.

[32] K. Takanashi and M. Nakashima, "Japanese activities on on-line testing," *Journal of Engineering Mechanics*, vol. 113, no. 7, pp. 1014–1032, 1987.

[33] D. P. Stoten and R. A. Hyde, "Adaptive control of dynamically substructured systems: the single-input single-output case," *Proceedings of the Institution of Mechanical Engineers - Part I: Journal of Systems & Control Engineering*, vol. 220, no. 2, pp. 63–79, 2006.

[34] A. S. Elnashai, A. Y. El-Ghazouli, and P. J. Dowling, "Verification of pseudo-dynamic testing of steel members," *Journal of Constructional Steel Research*, vol. 16, no. 2, pp. 153–161, 1990.

[35] M. Nakashima, H. Kato, and E. Takaoka, "Development of real-time pseudo dynamic testing," *Earthquake Engineering & Structural Dynamics*, vol. 21, no. 1, pp. 79–92, 1992.

[36] S. A. Mahin and P. B. Shing, "Pseudodynamic method for seismic testing," *Journal of Structural Engineering*, vol. 111, no. 7, pp. 1482–1503, 1985.

[37] M. Nakashima and N. Masaoka, "Real-time on-line test for MDOF systems," *Earthquake Engineering & Structural Dynamics*, vol. 28, no. 4, pp. 393–420, Article ID 199904, 1999.

[38] T. Horiuchi, M. Inoue, T. Konno, and Y. Namita, "Real-time hybrid experimental system with actuator delay compensation and its application to a piping system with energy absorber," *Earthquake Engineering & Structural Dynamics*, vol. 28, no. 10, pp. 1121–1141, Article ID 199910, 1999.

[39] T. Horiuchi and T. Konno, "A new method for compensating actuator delay in real–time hybrid experiments," *Philosophical Transactions of the Royal Society of London,Series A: Mathematical, Physical and Engineering Sciences*, vol. 359, no. 1786, pp. 1893–1909, 2001.

[40] A. P. Darby, M. S. Williams, and A. Blakeborough, "Stability and delay compensation for real-time substructure testing," *Journal of Engineering Mechanics*, vol. 128, no. 12, pp. 1276–1284, 2002.

[41] M. I. Wallace, J. Sieber, S. A. Neild, D. J. Wagg, and B. Krauskopf, "Stability analysis of real-time dynamic substructuring using delay differential equation models," *Earthquake Engineering & Structural Dynamics*, vol. 34, no. 15, pp. 1817–1832, 2005.

[42] R. Enokida, D. Stoten, and K. Kajiwara, "Stability analysis and comparative experimentation for two substructuring schemes, with a pure time delay in the actuation system," *Journal of Sound and Vibration*, vol. 346, no. 1, pp. 1–16, 2015.

[43] M. Ahmadizadeh, G. Mosqueda, and A. M. Reinhorn, "Compensation of actuator delay and dynamics for real-time hybrid structural simulation," *Earthquake Engineering & Structural Dynamics*, vol. 37, no. 1, pp. 21–42, 2008.

[44] C. Chen and J. M. Ricles, "Large-scale real-time hybrid simulation involving multiple experimental substructures and adaptive actuator delay compensation," *Earthquake Engineering & Structural Dynamics*, vol. 41, no. 3, pp. 549–569, 2012.

[45] L. Huang, C. Chen, T. Guo, and X. Gao, "Stability analysis of real-time hybrid simulation with time-varying delay through a delay decomposition approach," *Journal of Engineering Mechanics*, vol. 146, no. 10, Article ID 04020109, 2020.

[46] J. E. Carrion, B. F. Spencer, and B. M. Phillips, "Real-time hybrid simulation for structural control performance assessment," *Earthquake Engineering and Engineering Vibration*, vol. 8, no. 4, pp. 481–492, 2010.

[47] X. Gao and S. J. Dyke, "Modeling and control of actuators for high performance structural dynamic testing," *Smart Materials and Structures*, vol. 23, no. 5, Article ID 055008, 2014.

[48] J. Y. Tu, P. Y. Lin, D. P. Stoten, and G. Li, "Testing of dynamically substructured, base-isolated systems using adaptive control techniques," *Earthquake Engineering & Structural Dynamics*, vol. 56, pp. 661–681, 2009.

[49] J. Y. Tu, D. P. Stoten, R. A. Hyde, and G. Li, "A state-space approach for the control of multivariable dynamically substructured systems," *Proceedings of the Institution of Mechanical Engineers - Part I: Journal of Systems & Control Engineering*, vol. 225, no. 7, pp. 935–953, 2011.

[50] D. P. Stoten, "A comparative study and unification of two methods for controlling dynamically substructured systems," *Earthquake Engineering & Structural Dynamics*, vol. 46, no. 2, pp. 317–339, 2017.

[51] G. Li, D. Stoten, and J. Y. Tu, "Model predictive control of dynamically substructured systems with application to a servohydraulically actuated mechanical plant," *IET Control Theory & Applications*, vol. 4, no. 2, pp. 253–264, 2010.

[52] R. Ishibashi, K. Seki, and M. Iwasaki, "Feedback controller design based on H_∞ control theory in dynamically substructured system," in *Proceedings of the 2020 IEEE 16th International Workshop on Advanced Motion Control (AMC)*, September 2020.

[53] R. Enokida and K. Kajiwara, "Nonlinear signal-based control with an error feedback action for nonlinear substructuring control," *Journal of Sound and Vibration*, vol. 386, pp. 21–37, 2017.

[54] R. Enokida and K. Kajiwara, "Nonlinear substructuring control for parameter changes in multi-degree-of-freedom systems," *Journal of Sound and Vibration*, vol. 407, pp. 63–81, 2017.
[55] R. Enokida, "Basic examination of two substructuring schemes for shake table tests," *Structural Control and Health Monitoring*, vol. 27, no. 4, pp. 1–23, 2020.
[56] R. Enokida, "Nonlinear substructuring control for simultaneous control of acceleration and displacement in shake table substructuring experiments," *Structural Control and Health Monitoring*, vol. 29, no. 2, Article ID e2882, 2022.
[57] D. P. Stoten, "Fusion of kinetic data using composite filters," *Proceedings of the Institution of Mechanical Engineers - Part I: Journal of Systems & Control Engineering*, vol. 215, no. 5, pp. 483–497, 2001.
[58] A. R. Plummer, "Optimal complementary filters and their application in motion measurement," *Proceedings of the Institution of Mechanical Engineers - Part I: Journal of Systems & Control Engineering*, vol. 220, no. 6, pp. 489–507, 2006.